Acta Pharmaceutica Sinica B 2026;16(7):4654−4675

Chinese Pharmaceutical Association
Institute of Materia Medica, Chinese Academy of Medical Sciences

Acta Pharmaceutica Sinica B

www.elsevier.com/locate/apsb
www.sciencedirect.com

ORIGINAL ARTICLE

Enhanced tumor immunotherapy by nanovesicles derived from engineered DC-like M1 macrophage

Linxia Jiang[a,†], Yi Yan[a,†], Hongqian Xie[a], Zhiyi Xu[a], Xiaoru Guo[a], Jinyue Li[a], Xiaoyu Liu[a], Di Wu[a], Yuanjun Zhu[a,b], Yujie Shi[a], Xiaoyan Liu[a], Jian-Cheng Wang[a,b,c,*]

[a]*Beijing Key Laboratory of Molecular Pharmaceutics and New Drug Delivery Systems, State Key Laboratory of Natural and Biomimetic Drugs, School of Pharmaceutical Sciences, Peking University, Beijing 100191, China*
[b]*Laboratory of Innovative Formulations and Pharmaceutical Excipients, Ningbo Institute of Marine Medicine, Peking University, Ningbo 315832, China*
[c]*Beijing Advanced Center of Cellular Homeostasis and Aging-Related Diseases, Institute of Advanced ClinicaMedicine, Peking University, Beijing 100191, China*

Received 29 August 2025; received in revised form 19 October 2025; accepted 7 November 2025

KEY WORDS

Nanovesicles;
PIB transcription factors;
Cell reprogramming;
Dendritic cells;
$CD8^+$ T cell activation;
Tumor-associated macrophages;
Tumor immunotherapy;
Immunomodulatory enhancer

Abstract To explore a therapeutic approach with dual functions of activating cytotoxic $CD8^+$ T cells and remodeling immunosuppressive tumor-associated macrophages (TAMs), the engineered macrophage-derived nanovesicles (MAC-PNV) were developed in this study. The MAC-PNV were derived from activated DC-like M1 macrophages after reprogramming macrophages by transcription factors PIB (PU.1, IRF8, and BATF3) and further stimulated with antigenic peptide, lipopolysaccharide (LPS), and interferon-γ (IFN-γ). *In vitro* results demonstrated that the enriched antigen-presenting complexes and co-stimulatory molecules were displayed on the surface of pro-inflammatory cargo-contained MAC-PNV, which enabled significant activation of $CD8^+$ T cells and repolarization of M2 macrophages towards the M1 phenotype. After peritumoral administration, MAC-PNV alone significantly inhibited tumor growth by promoting the activation and intra-tumoral infiltration of $CD8^+$ T cells, and remodeling the immunosuppressive tumor microenvironment (TME) in B16-OVA-bearing mouse models. More importantly, MAC-PNV remarkably enhanced the anti-tumor efficacy of low-dose liposomal doxorubicin

*Corresponding author.
E-mail address: wang-jc@bjmu.edu.cn (Jian-Cheng Wang).
[†]These authors made equal contributions to this work.
Peer review under the responsibility of Chinese Pharmaceutical Association and Institute of Materia Medica, Chinese Academy of Medical Sciences.

https://doi.org/10.1016/j.apsb.2025.12.029

(DOX-Lipo, 1 mg/kg), along with reducing its dose-limiting toxicities in B16-F10-bearing mouse models. This study highlights that the MAC-PNV would be a potential and effective immunomodulatory enhancer for providing a promising combination strategy with clinical chemotherapeutics.

1. Introduction

Tumor immunotherapy has emerged as a promising tumor treatment strategy and achieved remarkable efficacy in clinical practice[1]. As is known to all, cytotoxic $CD8^+$ T cells are the most powerful effectors for robust anti-tumor immunotherapy[2-4]. Unfortunately, intra-tumoral infiltration and cytotoxic activity of $CD8^+$ T cells are always impeded by the immunosuppressive tumor microenvironment (TME) in solid tumors[5], where M2-phenotype tumor-associated macrophages (TAMs) secrete immunosuppressive cytokines, including interleukin-10 (IL-10) and transforming growth factor-β (TGF-β)[6,7]. Therefore, exploring a therapeutic approach with dual functions of activating cytotoxic $CD8^+$ T cells and remodeling immunosuppressive TAMs is crucial for improving anti-tumor immunotherapy.

Dendritic cells (DCs) are recognized as the most potent professional antigen-presenting cells (APCs) that can cross-present tumor antigens to $CD8^+$ T cells for initiating cytotoxic T cell responses[8]. Given the pivotal role of DCs in driving immune responses, Pereira et al.[9-11] developed DC-like tumor cells or fibroblasts with the approach of transcription factor combinations (PU.1, IRF8, and BATF3, abbreviated as PIB), which endowed tumor cells or fibroblasts with antigen presentation capability. Mechanistically, PU.1, as a pioneer transcription factor, showed dominant and independent chromatin targeting at early phases of reprogramming. It subsequently recruited IRF8 and BATF3 to shared binding sites. The cooperative binding at open enhancers and promoters led to activation of a DC transcriptional program[12]. These reprogrammed DC-like cells exhibited the expression of antigen presentation complexes and co-stimulatory molecules, thereby improving their capability to prime $CD8^+$ T cell responses[9,10]. In addition, M1 macrophages mediate potent pro-inflammatory and anti-tumor effects through the inflammatory component (*e.g.*, tumor necrosis factor-α (TNF-α), interleukin-6 (IL-6), and inducible nitric oxide synthase)[13,14]. Recent studies had demonstrated that the M1 macrophage-derived nanovesicles (NVs) could facilitate the repolarization of M2 TAMs towards M1 phenotypes, thereby ameliorating immunosuppression of TME[15-17]. Inspired by these findings, we hypothesized that transcription factor combinations would endow M1 macrophages with DC-like phenotype, along with retaining the identity of M1 macrophages. These reprogrammed M1 macrophage-derived NVs might possess the dual functions of activating $CD8^+$ T cells and remodeling TAMs.

In this study, the engineered macrophage-derived nanovesicle (MAC-PNV) was developed. As shown in Fig. 1, DC-like macrophages (DC-like M) were generated through reprogramming macrophages with the forced expression of PIB. Subsequently, activated DC-like M1 macrophages (aDC-like M1) were acquired after treatment with tumor antigenic peptide, lipopolysaccharide (LPS), and interferon-γ (IFN-γ). Then, aDC-like M1-derived nanovesicle (MAC-PNV) was produced by sequential extrusion and gradient centrifugation. After peritumoral administration, MAC-PNV promoted repolarization of M2 TAMs towards M1 phenotype, releasing pro-inflammatory factors to reverse the immunosuppressive TME. In addition, MAC-PNV directly activated $CD8^+$ T cells within tumor-draining lymph nodes (TDLNs), thereby inducing robust anti-tumor immune responses. Furthermore, to verify the potential of MAC-PNV for enhancing the therapeutic efficacy and reducing the dose-limiting toxicity of clinical anti-tumor therapeutics, the effects and safety profile of combining MAC-PNV with low-dose liposomal doxorubicin (DOX-Lipo) were assessed in mouse models bearing B16-OVA or B16-F10 tumors.

2. Materials and methods

2.1. Reagents

Doxorubicin hydrochloride (DOX) was purchased from MREDA Technology (Beijing, China). Lipofectamine 3000, Quant-iT Ribogreen assay kit, and eBioscience™ Foxp3/Transcription Factor Staining Buffer Set were purchased from Thermo Fisher Scientific (Waltham, MA, USA). $OVA_{257-264}$ and NATE™ were purchased from Invivogen (Toulouse, France). The plasmids of pCMV and pCMV-PIB were purchased from Ruibiotech Co., Ltd. (Beijing, China). DMEM and RPMI-1640 medium were purchased from Macgene Technology Co., Ltd. (Beijing, China). Recombinant Murine GM-CSF, IL-4, and M-CSF were purchased from PeproTech (Waltham, MA, USA). EndoFree Plasmid Maxi Kit was purchased from QIAGEN (Hilden, Germany). Nuclepore™ Track-Etch Membranes (5, 1, 0.4, and 0.2 μm) were purchased from Whatman (Kent, UK). Carboxyfluorescein succinimidyl ester (CFSE) was purchased from Tonbo Biosciences (San Diego, CA, USA). LDH Cytotoxicity Assay Kit was purchased from Beyotime Biotechnology (Nanjing, China). Mouse IFN-γ ELISA kit, mouse IL-2 ELISA kit, and mouse TNF-α ELISA kit were purchased from Dakewe Biotech Co., Ltd. (Shenzhen, China). Mouse IL-6 ELISA kit was purchased from Dongge Boye Biotechnology Co., Ltd. (Beijing, China). PU.1 antibody, IRF8 antibody, CD80 antibody, and MHC-I antibody were purchased from Cell Signaling Technology (Boston, MA, USA). CD86 antibody was purchased from ProteinTech Group (Chicago, IL, USA). BATF3 antibody was purchased from EbioCell Lifesciences (Durham, UK). PE anti-mouse CD44, FITC anti-mouse CD69, Brilliant Violet 421™ anti-mouse CD11b, PE anti-mouse H-2Kb bound to SIINFEKL, FITC anti-mouse F4/80, FITC anti-mouse CD3, PerCP/Cyanine5.5 anti-mouse CD4, FITC anti-mouse CD11c, APC anti-mouse CD45, APC anti-mouse CD86, PE anti-mouse CD206 (MMR), PE/Cyanine7 anti-mouse CD8a, PE anti-mouse IFN-γ, PE anti-mouse PU.1, and PE/Cyanine7 anti-mouse CD80 were purchased from BioLegend (San Diego, CA, USA). The miDETECT A Track™ miRNA

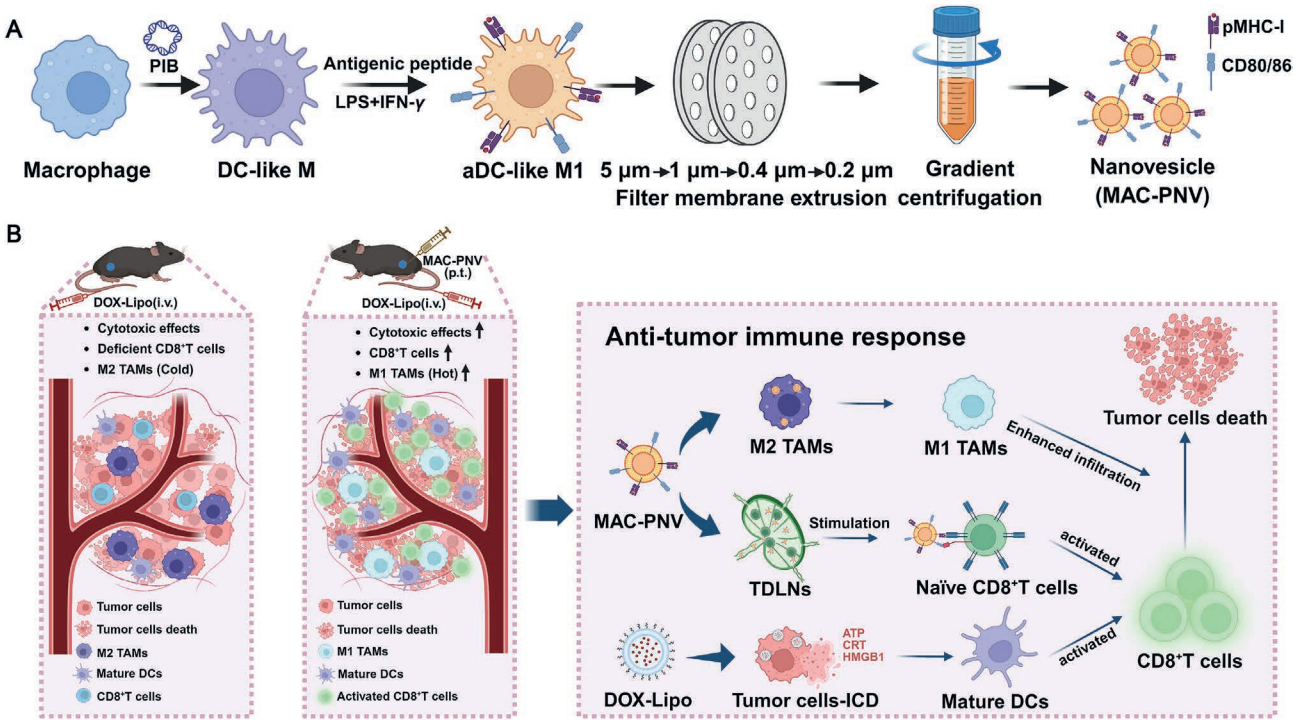

Figure 1 Preparation and anti-tumor mechanism of MAC-PNV. Activated DC-like M1 macrophage (aDC-like M1)-derived nanovesicles (MAC-PNV) were generated from engineered macrophages that were transfected with PIB plasmid and sequentially stimulated with antigenic peptides, lipopolysaccharide (LPS), and interferon-γ (IFN-γ). After peritumoral injection (p.t.), MAC-PNV passively drained to tumor-draining lymph nodes (TDLNs) to directly activate $CD8^+$ T cells. Concurrently, MAC-PNV retained at the tumor site promoted tumor-associated macrophages (TAMs) repolarization from immunosuppressive M2 phenotype to immunostimulatory M1 phenotype. Furthermore, when combined with the low dose of immunogenic cell death (ICD) inducer liposomal doxorubicin (DOX-Lipo, 1 mg/kg), MAC-PNV synergistically amplified anti-tumor immune responses to enhance therapeutic efficacy. Created with BioRender (https://biorender.com/).

RT-qPCR Starter Kit was purchased from Guangzhou Ruibo Biotechnology Co., Ltd. (Guangzhou, China).

2.2. *Cell culture*

B16-OVA cells or B16-F10 cells were obtained from MeisenCTCC (Hangzhou, China). The cells were cultured in DMEM medium supplemented with FBS (10%), penicillin (100 U/mL), and streptomycin (0.1 mg/mL) at 37 °C in a humidified atmosphere containing 5% CO_2.

Bone marrow-derived dendritic cells (BMDCs) and macrophages (BMDMs) were harvested from femurs and tibias of C57BL/6J mice (6−8 weeks, male). After euthanasia, the femurs and tibias of the mice were collected and soaked in 75% ethanol for 3 min. Following removal of the ends of bones, the marrow was flushed with PBS using a sterile syringe (1 mL). The collected suspension was treated with erythrocyte lysis solution and filtered through a 70 μm filter. For BMDCs differentiation, the cells were resuspended in RPMI-1640 medium supplemented with GM-CSF (10 ng/mL), IL-4 (10 ng/mL), FBS (10%), penicillin (100 U/mL) and streptomycin (0.1 mg/mL), and then seeded in 6-well plates at 8×10^6 cells per well. On Days 2 and 4, half of the medium was removed and supplemented with fresh medium containing cytokines. The BMDCs were harvested on Day 6[18]. For BMDMs differentiation, the cells were resuspended in DMEM medium supplemented with M-CSF (20 ng/mL), FBS (10%), penicillin (100 U/mL), and streptomycin (0.1 mg/mL), and then seeded in 6-well plates at 3×10^6 cells per well. The medium was replaced with fresh cytokine-containing medium on Days 3 and 6. The BMDMs were harvested on Day 7[19].

To extract peritoneal macrophages (PEMs), C57BL/6J mice (6−8 weeks, male) were intraperitoneally injected with 1 mL of 3% brewer thioglycolate medium. After 72 h, mice were euthanized and subjected to peritoneal lavage with ice-cold RPMI-1640 medium. The lavage fluid was centrifuged, and the cells were resuspended in RPMI 1640 medium supplemented with FBS (10%), penicillin (100 U/mL), and streptomycin (0.1 mg/mL). These cells were seeded in 6-well plates at a density of 1×10^6 per well for subsequent experiments[20].

2.3. *Animals*

C57BL/6J mice (6−8 weeks, male) were purchased from Beijing Vital River Laboratory Animal Technology Co., Ltd. (Beijing, China). OT-I mice were purchased from The Jackson Laboratory. All animal care and experiments were conducted following the approval of the Institutional Authority for Laboratory Animal Care of Peking University (Approval No. LA2021499).

2.4. *Preparation and characterization of activated DC-like M1 macrophage*

PU.1, IRF8, and BATF3 (PIB) transcription factors were expressed in a polycistronic structure, and the coding sequence of

PIB was cloned into the pCMV plasmid with a 2A self-cleaving peptide as an interval. The empty pCMV was used as a control throughout the experiment. PEMs were transfected with PIB plasmid using Lipofectamine 3000 according to the manufacturer's protocol on Days 0, 2, 4, and 6, and NATE™ transfection enhancer was added to improve transfection efficiency. To evaluate the transfection efficiency of the PIB plasmid, PEMs were harvested on Day 7 after transfection with the PIB plasmid, and then treated with the Transcription Factor Staining Buffer Set. The cells were subsequently labeled with different fluorescent antibodies. PU.1 was stained using the PE-conjugated anti-mouse PU.1 antibody, while IRF8 was stained with a primary anti-IRF8 antibody followed by a FITC-conjugated secondary antibody. After that, the cells were washed with PBS, harvested, and then analyzed by flow cytometry to determine the percentages of PU.1- and IRF8-positive populations. In addition, the cell viability of PEMs was detected using the CCK-8 assay on Day 7 after transfection with the PIB plasmid.

To assess the reprogramming efficiency of DC-like macrophage (DC-like M), the cells were stained with FITC anti-mouse CD11c and PE/Cyanine7 anti-mouse MHC-II antibodies on Days 5, 7, and 9 after transfection of PEMs with PIB plasmid. The percentage of $CD11c^+$ $MHC\text{-}II^+$ cells was evaluated by flow cytometry. In addition, macrophage phenotype was analyzed through staining cells with FITC anti-mouse F4/80 and Brilliant Violet 421™ anti-mouse CD11b antibodies.

To further construct an activated DC-like M1 macrophage (aDC-like M1), PEMs were transfected with the PIB plasmid on Days 0, 2, 4, and 6. The DC-like M were harvested on Day 7 and then treated with antigenic peptide ($OVA_{257-264}$: 10 μg/mL, or $TRP2_{181-188}$: 20 μmol/L), LPS (1 μg/mL), and IFN-γ (20 ng/mL) for 24 h to obtain aDC-like M1. To evaluate the antigen presentation capability of aDC-like M1, cells were stained with PE anti-mouse H-2Kb bound to SIINFEKL, APC anti-mouse CD86, and PE/Cyanine7 anti-mouse CD80 antibodies. The percentages of $CD80^+CD86^+$ and $SIINFEKL\text{-}H\text{-}2Kb^+$ population in aDC-like M1 were analyzed by flow cytometry (CytoFLEX LX, Beckman Coulter, Indianapolis, IN, USA). To confirm the M1 phenotype of aDC-like M1, mRNA expression levels of the *INOS* and *IL6* (M1 markers) were assessed using RT-qPCR. Total RNA was extracted from aDC-like M1 using TRIZOL® reagent (Invitrogen, Carlsbad, CA, USA), followed by reverse transcription using the GoScript™ Reverse Transcription System (Promega, Madison, WI, USA). Quantitative PCR amplification was performed using GoTaq®qPCR Master Mix (Promega, Madison, WI, USA) on a CFX Connect Real-Time PCR system (Bio-Rad, Hercules, CA, USA). *GAPDH* served as the reference gene for mRNA normalization. The sequences of RT-qPCR primers were shown in Supporting Information Table S1. The relative mRNA expression levels were calculated by $2^{-\Delta\Delta Ct}$ method.

2.5. Preparation and characterization of NVs

The aDC-like M1-derived nanovesicles (MAC-PNV) were prepared *via* sequential extrusion and gradient centrifugation. Briefly, aDC-like M1 were washed twice with PBS to remove cell debris and residual culture medium. These cells were collected and resuspended in PBS at 5×10^6 cells/mL, then sequentially extruded through polycarbonate membranes (with pore sizes of 5, 1 μm, 400, and 200 nm, respectively) using a mini-extruder to prepare MAC-PNV. MAC-PNV were further purified through gradient centrifugation (2000×*g* for 10 min to remove cell debris, 8000×*g* for 15 min to remove large vesicles, and 120,000×*g* for 90 min to obtain NVs). The prepared MAC-PNV was resuspended in cold PBS and stored at −80 °C.

PEMs were transfected with an empty plasmid on Days 0, 2, 4, and 6 and harvested on Day 7. Then the cells were treated with antigenic peptide ($OVA_{257-264}$: 10 μg/mL), LPS (1 μg/mL), and IFN-γ (20 ng/mL) for 24 h to obtain $_{VM1}PEM_{OVA}$ ($_{VM1}PEM_{OVA}$: PEM transfected with empty plasmid prior to stimulation with LPS, IFN-γ, and $OVA_{257-264}$). The $_{VM1}PEM_{OVA}$-derived NV (MAC-CNV) was prepared according to the above method. In addition, DC-NV were derived from activated BMDC (aBMDC), which were obtained after treating BMDC with $OVA_{257-264}$ (10 μg/mL), LPS (1 μg/mL), and IFN-γ (20 ng/mL) for 24 h.

The average particle size and zeta potential of NVs were determined using a dynamic light scattering (DLS) particle size analyzer (Zetasizer Nano-ZS90, Malvern Instruments Ltd., UK). The morphology of NVs was observed by transmission electron microscopy (TEM, JEM-1400 plus, JEOL Ltd., Japan) after staining NVs with 2% sodium phosphotungstate solution on carbon-coated copper grids. The stability of NVs was evaluated by monitoring changes in particle size following 5-day storage at 4 °C, and by assessing changes in both particle size and total protein content after one-month storage at −80 °C. The yield of NVs was quantified by measuring the total protein content of NVs derived from a defined number of parent cells. The protein recovery rate was calculated using Eq. (1):

$$\text{Protein recovery rate (\%)} = (\text{Total protein content of nanovesicles/Total protein content of the parent cells}) \times 100 \quad (1)$$

The presence of proteins in NVs was detected by Western blotting. The protein concentration of NVs was quantified using a BCA protein quantification kit according to the manufacturer's protocol. The proteins were separated by 10% sodium dodecyl sulfate polyacrylamide gel electrophoresis and transferred onto a PVDF membrane (Pall, New York, NY, USA). After blocking with 5% skim milk solution for 1 h at room temperature, the membrane was incubated with primary antibodies against MHC-I, CD80, CD86, CD9, CD81, TSG101, or Alix (1:1000) overnight at 4 °C[21], and then incubated with a horseradish peroxidase (HRP)-labeled secondary antibody at room temperature for 2 h. The protein bands were visualized using the Amersham Imager 600 system (GE Healthcare Life sciences, Marlborough, MA, USA) after treatment with enhanced chemiluminescence (ECL) (Merck Millipore, Darmstadt, Germany). Antigen-presenting-related proteins of NVs were quantified using LC−MS/MS. Raw data files were analyzed using Proteome Discoverer (PD) software (version 2.4, Thermo Fisher Scientific, Waltham, MA, USA).

The relative mRNA and miRNA contents of NVs were quantified by RT-qPCR. Total RNA was extracted from NVs using TRIZOL® reagent, followed by reverse transcription using the GoScript™ Reverse Transcription System. Quantitative PCR amplification was performed using GoTaq®qPCR Master Mix on a CFX Connect Real-Time PCR system (Bio-Rad, Hercules, CA, USA). *GAPDH* served as the reference gene for mRNA normalization. The sequences of RT-qPCR primers are shown in Table S1. The relative mRNA expression levels were calculated by $2^{-\Delta\Delta Ct}$ method. In addition, the miDETECT A Track™ miRNA RT-qPCR Starter Kit (RiboBio, Guangzhou, China) was used to quantify the relative content of miRNA according to the manufacturer's protocol. *U6* was used as the endogenous control gene.

2.6. Preparation and characterization of liposomal doxorubicin

Liposomal doxorubicin (DOX-Lipo) was prepared by the ammonium sulfate gradient method. Briefly, hydrogenated soy phosphatidylcholine (HSPC), cholesterol, and distearoyl phosphatidylethanolamine-polyethylene glycol 2000 (DSPE-PEG_{2000}) were dissolved in chloroform at a molar ratio of 65:30:5, and then the organic solvent was removed by rotary evaporation to yield a thin lipid film. The film was hydrated with 120 mmol/L ammonium sulfate. The hydrated lipids were subjected to intermittent probe sonication for 5 min to obtain blank liposomes. The external medium of the liposomes was replaced with PBS by dialysis method, and then DOX was loaded into the liposomes at 60 °C. Free DOX was removed by ultracentrifugation. The particle size and zeta potential of DOX-Lipo were determined by DLS. Encapsulation rate and drug loading of DOX were determined by a UV spectrophotometer[22].

2.7. In vitro $CD8^+$ T cells proliferation and activation assay

To evaluate the capability of NVs to directly activate naïve $CD8^+$ T cells, $CD8^+$ T cells were isolated from the spleens of OT-I mice. Splenocytes were stained with APC anti-mouse CD3 and PE/Cyanine7 anti-mouse CD8a antibodies. Then, $CD8^+$ T cells were purified by flow cytometric cell sorting (FACS). Sorted OT-I $CD8^+$ T cells (1×10^5 per well) were cultured with NVs (10 μg/mL of total protein) for 72 h. The cell supernatant was collected to determine concentrations of IFN-γ, IL-2, and TNF-α using ELISA kits according to the manufacturer's protocols. The $CD8^+$ T cells were collected to analyze the expression of CD69 and CD44 on the surface by flow cytometry. Furthermore, to assess the proliferation ability of $CD8^+$ T cells, OT-I $CD8^+$ T cells were labeled with CFSE and then co-cultured with NVs (10 μg/mL of total protein) in 96-well plates (1×10^5 per well) for 72 h. The proliferation ability of the $CD8^+$ T cells was detected by flow cytometry.

2.8. Analysis for in vitro tumor killing efficiency of $CD8^+$ T cells

The killing efficiency of activated $CD8^+$ T cells against B16-OVA tumor cells was evaluated by the lactate dehydrogenase (LDH) assay kit. Briefly, activated $CD8^+$ T cells were harvested after different treatments and co-cultured with B16-OVA cells at effector-to-target (E:T) ratios of 1:1, 5:1, and 10:1 for 24 h. The cell supernatants were collected, and the levels of LDH were measured according to the manufacturer's instructions. In addition, the viability of B16-OVA cells was assessed by MTT assay. Briefly, the above co-cultured cells were washed three times with PBS, followed by incubation with 200 μL of serum-free medium (containing 5 mg/mL MTT) for 4 h at 37 °C. Then, DMSO solution (100 μL) was added after the removal of the cell medium. Absorbance was measured at 570 nm using a microplate meter (Varioskan LUX, Thermo Fisher scientific, Waltham, MA, USA).

2.9. Macrophage repolarization analysis

PEMs were seeded in 12-well plates (5×10^5 cells per well) and polarized into M2 phenotype following stimulation with IL-4 (20 ng/mL) for 24 h. These M2 macrophages were then treated with DC-NV, MAC-CNV, and MAC-PNV (100 μg/mL of total protein) for 24 h. The repolarization efficiency of macrophages was evaluated using flow cytometry and RT-qPCR. The cells were incubated with CD86 antibody (M1 marker) and CD206 antibody (M2 marker). The $CD86^+$ population and $CD206^+$ population in macrophages were analyzed using flow cytometry. The mRNA expression levels of M1 markers (*IL12* and *IL6*) and M2 markers (*CD206* and *ARG1*) were detected by RT-qPCR. In addition, the supernatants of these cells were collected, and the expression levels of TNF-α, IFN-γ, nitric oxide (NO), and CXCL10 were detected by ELISA kits and the NO assay.

For the phagocytosis assay, IL-4-stimulated PEMs (as M2 macrophages) were treated with NVs for 24 h. These macrophages (1×10^5 cells per well) were then co-cultured with CFSE-labeled B16-F10 tumor cells (2×10^5 cells per well) for 12 h. After that, all cells were collected and stained with Brilliant Violet 421™ anti-mouse CD11b antibody. The percentage of $CFSE^+$ $CD11b^+$ population was determined using flow cytometry to evaluate macrophage phagocytic activity. In addition, to evaluate the $CD8^+$ T cell-activating capacity of repolarized macrophages, M2 macrophages (5×10^4 cells) were pulsed with $OVA_{257-264}$ and then co-cultured with CFSE-labeled OT-I $CD8^+$ T cells (1×10^5 cells) in 96-well plates for 72 h. The proliferation rate of $CD8^+$ T cells was detected by flow cytometry.

The cargo of MAC-PNV was eliminated through the treatment of saponin, as reported in literatures[23,24]. Briefly, MAC-PNV was mixed with an equal volume of 0.2% *w/v* saponin and incubated at room temperature for 30 min[24]. Then the samples were washed twice with sterile PBS and centrifuged at 120,000×*g* for 90 min to collect the NVs. Quant-iT Ribogreen assay kit (Thermo Fisher scientific, Waltham, MA, USA) and BCA protein quantification kit were used to evaluate the elimination efficiency of RNA and protein by saponins, respectively, according to the manufacturer's instructions.

2.10. In vivo biodistribution assay

Cy7-labeled NVs were prepared by mixing NVs (1 mg/mL of total protein) with 200 μmol/L DSPE-Cy7 (dissolved in ethanol) at a 9:1 volume ratio and then co-extruding through a 200 nm polycarbonate membrane, followed by incubation at room temperature for 30 min. The labeled NVs were then collected *via* ultracentrifugation (120,000×*g*, 90 min) to remove unincorporated dye. B16-OVA cells (2.0×10^5 cells per mouse, 100 μL) were subcutaneously (s.c.) implanted into the right flank of C57BL/6 mice (6−8 weeks, male). When the tumor volume reached about 400−600 mm^3, Cy7-labeled NVs were peritumorally injected into mice. *In vivo* fluorescence images were observed using an *in vivo* imaging system (IVIS Spectrum, PerkinElmer, Waltham, MA, USA) at predetermined time points (excitation and emission wavelengths of 748 and 780 nm). All images were analyzed using Living Image software.

2.11. In vivo anti-tumor assay

For the primary tumor model, B16-OVA cells (2.0×10^5 cells per mouse, 100 μL) were subcutaneously (s.c.) injected on the right flank of male C57BL/6 mice. After 7 days, the tumor volume had reached about 50−100 mm^3, PBS, DC-NV, MAC-CNV, or MAC-PNV (1 mg/mL of total protein, 100 μL per mouse) were injected peritumorally on the 7th, 10th, and 13th days, respectively. Tumor volume and body weight of the treated mice were measured every 2 days. The tumor volume was calculated according to Eq. (2):

$$\text{Tumor volume} = (\text{Tumor length}) \times (\text{Tumor width})^2 \times 0.5 \quad (2)$$

After the mice were euthanized on the 18th day, the tumors were extracted, photographed, and weighed. TDLNs and tumor

tissues were harvested for flow cytometry analysis of *in vivo* immune cells. Major organs (heart, liver, spleen, lung, and kidney) were harvested for safety evaluation.

For bilateral B16-OVA tumor-bearing mice, B16-OVA tumor cells (2.0×10^5 cells per mouse, 100 μL) were inoculated (s.c.) into the right and left flanks of C57BL/6 mice on Days 0 and 3, respectively. PBS, DC-NV, MAC-CNV, or MAC-PNV (1 mg/mL of total protein, 100 μL per mouse) were injected peritumorally on the right side on the 7th, 10th, and 13th days, respectively. The bilateral tumor volume of the mice was monitored every 2 days. On the 18th day, the mice were euthanized. Bilateral tumors were harvested, photographed, and weighed. The tumor tissues and spleens of the mice were harvested for flow cytometry analysis.

To investigate the anti-tumor effects of MAC-PNV combined with DOX-Lipo, B16-OVA tumor-bearing mice (tumor volume 50−100 mm^3) were randomly divided into PBS, DOX-Lipo, MAC-PNV, and MAC-PNV + DOX-Lipo groups. For B16-F10 tumor-bearing mice models, B16-F10 cells (2.0×10^5 cells per mouse, 100 μL) were subcutaneously (s.c.) injected on the right flank of male C57BL/6 mice. When the tumor volume reached about 50−100 mm^3, the mice were randomly divided into PBS, DOX-Lipo(L), DOX-Lipo, MAC-PNV_{TRP2}, MAC-PNV_{TRP2}+DOX-Lipo(L), and MAC-PNV_{TRP2}+DOX-Lipo groups. MAC-PNV or MAC-PNV_{TRP2} (1 mg/mL of total protein, 100 μL per mouse) was injected peritumorally, and DOX-Lipo(L) (1 mg/kg) or DOX-Lipo (3 mg/kg) was injected intravenously on the 7th, 10th, and 13th days. The body weight and tumor volume of mice were measured during the treatment. The mice were euthanized on Day 20 or 22. The tumor tissues and TDLNs of the mice were collected for flow cytometry analysis.

For the B16-OVA lung metastases model, B16-OVA cells (2.5×10^5 cells per mouse) were intravenously inoculated into male C57BL/6 mice, along with inoculated (2.0×10^5 B16-OVA cells per mouse, 100 μL, s.c.) into the right flank of mice. On the 7th, 10th, and 13th days, MAC-PNV (1 mg/mL of total protein, 100 μL per mouse) was peritumorally injected, and DOX-Lipo (3 mg/kg) was intravenously injected. On the 23rd day, the mice were euthanized. Lung tissues of mice were collected and fixed with Bouin's solution. The lung metastatic nodules were quantified and stained with hematoxylin & eosin (H&E).

2.12. Evaluation of in vivo immune responses

The *ex vivo* tumor tissues, TDLNs, and spleens of mice were dissociated into single-cell suspensions *via* mechanical grinding followed by filtering with a 70 μm filter. Erythrocyte lysate was added to the single-cell suspensions and incubated for 5 min to remove red blood cells. The cells were then washed with PBS and centrifuged at 1500 rpm (3K15, Sigma, Osterode, Germany) for 5 min. The collected cells (1×10^6 cells) were resuspended in 200 μL of ice-cold PBS and incubated with Fixable Viability Dye eFluor™ 506 (eBioscience™) for dead cell exclusion. After that, the cells were treated with the anti-CD16/32 antibody to block Fc receptors. Then, different cell suspensions were stained with different antibodies in the dark according to the manufacturer's suggested concentration. For $CD8^+$ T cell analysis, the cells in tumors and TDLNs were stained with FITC-anti-mouse CD3, APC-anti-mouse CD45, and PE/Cyanine7-anti-mouse CD8a antibodies. To investigate the percentage of IFN-γ^+CD8^+ T cells in the spleen and tumors, the cells were incubated with cell stimulation cocktail (containing protein transport inhibitors) for 6 h at 37 °C, and then stained with FITC-anti-mouse CD3, APC-anti-mouse CD45, PE/Cyanine7-anti-mouse CD8a, and PE-anti-mouse IFN-γ antibodies. For Tregs analysis, the cells in tumors were stained with APC anti-mouse CD45, PerCP/Cyanine5.5 anti-mouse CD4, APC anti-mouse CD25, and PE anti-mouse Foxp3 antibodies. To evaluate the polarization efficiency of TAMs in tumors, the cells of tumor tissues were stained with BV421-anti-mouse CD11b, FITC-anti-mouse F4/80, PE-anti-mouse CD206, and APC-anti-mouse CD86 antibodies. To quantify the percentage of mature DCs, cell suspensions obtained from TDLNs were stained with FITC-anti-mouse CD11c, PE anti-mouse H-2Kb bound to SIINFEKL, PE/Cyanine7-anti-mouse CD80, and APC-anti-mouse CD86 antibodies. Following stained with different antibodies for 30 min, cells were washed with PBS and harvested for flow cytometry analysis.

For ELISA analysis, tumor tissue homogenates were centrifuged at 12,000×*g* for 15 min at 4 °C. The concentrations of TNF-α, IL-6, and IFN-γ in the supernatants were detected by ELISA kits according to the manufacturer's protocols.

For immunofluorescence staining, *ex vivo* tumor tissues were sectioned and incubated with primary antibody and fluorescently labeled secondary antibody. Stained sections were observed using the quantitative pathology imaging system (Vectra Polaris, PerkinElmer, Waltham, MA, USA).

2.13. In vivo biosafety evaluation

The body weight of mice was measured every two days during the whole treatment. For histology analysis, major organs (heart, liver, spleen, lung, and kidney) were harvested, sectioned, stained with H&E, and then observed using the Digital pathology slide scanner (Buchi, Flawil, Switzerland). For the blood routine test, blood samples of mice were collected to measure the concentrations of red blood cells (RBC), platelets (PLT), hemoglobin (HGB), white blood cells (WBC), and lymphocytes (Lym) at the end of the treatment. For biochemical analysis, blood samples were collected under non-anticoagulation conditions and centrifuged at 3000 rpm (3K15, Sigma, Osterode, Germany) for 10 min at 4 °C. The serum was then collected to measure the levels of LDH, creatine kinase (CK), alanine aminotransferase (ALT), aspartate aminotransferase (AST), creatinine (CREA), and UREA. In addition, the concentrations of TNF-α and IL-6 in the serum were detected by ELISA kits according to the manufacturer's protocols.

2.14. Statistical analysis

Data are represented as mean ± standard deviation (Mean ± SD). Unpaired student's *t*-test was used for statistical analysis between two groups. Analysis of variance (ANOVA) was used for statistical analysis among multiple groups. Statistical significance was defined as $^*P < 0.05$, $^{**}P < 0.01$, and $^{***}P < 0.001$. All statistical analysis were carried out by SAS.

3. Results and discussion

3.1. Reprogramming macrophages into aDC-like M1

DCs are professional APCs that play pivotal roles in antigen recognition, processing, and presentation to activate T cells, particularly cross-presenting tumor antigens to $CD8^+$ T cells, thereby eliciting anti-tumor immunity[25]. In contrast, the capability of macrophages to activate $CD8^+$ T cells is far inferior to that of

DCs[26]. As reported in the previous study, both monocyte-derived DCs (mo-DCs) and monocyte-derived macrophages (mo-Macs) could efficiently cross-present antigens, but only mo-DCs could provide sufficient co-stimulatory signals for effective $CD8^+$ T cell activation[26]. It was due to the higher expression of co-stimulatory molecules (*e.g.*, CD80, CD86, and CD83) in mo-DCs compared to mo-Macs[26].

Herein, to verify the different expression levels of antigen-presenting molecules and co-stimulatory molecules among bone marrow-derived DC (BMDC), peritoneal macrophage (PEM), and bone marrow-derived macrophage (BMDM), LC−MS/MS and RT-qPCR were used to analyze the related proteins (*e.g.*, MHC-I, CD80, CD86, CD82, and CD83) and mRNAs (*H2KB*, *CD80*, and *CD86*). As shown in Fig. 2A and Supporting Information Fig. S1, comparable levels of MHC-I-related proteins and mRNAs were detected among the three cell types. Notably, significantly higher levels of multiple co-stimulatory molecules (CD80, CD86, CD82, and CD83) were found in BMDC than those in PEM and BMDM (Fig. 2A). Consistently, RT-qPCR results also demonstrated a significant upregulation of *CD8*0 mRNA (7.11- and 10.18-fold) and *CD8*6 mRNA (4.10- and 11.19-fold) in BMDC relative to BMDM and PEM (Fig. S1). Additionally, compared to PEM and BMDM, BMDC exhibited higher levels of CCR7 (Fig. 2A), which is a chemokine receptor related to the lymph node-homing ability of DCs[27]. No significant differences were observed in expression levels of other chemokine receptors (*e.g.*, CCR1 and CCR4) and cell adhesion molecules (*e.g.*, ICAM2 and SCAM1) among BMDC, PEM, and BMDM. Given the essential roles of MHC-I and co-stimulatory molecules (*e.g.*, CD80 and CD86) in $CD8^+$ T cell activation[28], we believed that the relatively low expression of co-stimulatory molecules in macrophages likely led to their insufficient $CD8^+$ T cell activation compared to DCs. Therefore, we proposed that the engineered macrophages with expression of DC-like co-stimulatory molecules would induce sufficient $CD8^+$ T cell activation.

As a proof of concept, PIB overexpression might confer macrophages with a DC-like phenotype to enhance their capability of $CD8^+$ T cell activation. In this study, an engineered DC-like macrophage (DC-like M) was prepared by transfecting PEMs with a PIB-encoding plasmid. As shown in Fig. 2B, the expressions of PU.1, IRF8, and BATF3 proteins were significantly upregulated in PIB-transfected PEM (PIB group) compared to vector-transfected PEM (vPEM group). The vPEM group referred to PEM transfected with an empty plasmid. Consistently, RT-qPCR results also confirmed significant upregulation of *PU.1*, *IRF8*, and *BATF3* mRNA in PIB group (Supporting Information Fig. S2). In addition, the percentages of PU.1-positive population and IRF8-positive population in PEMs were detected by flow cytometry on the 7th day after transfection with the PIB-encoding plasmid. As shown in Supporting Information Fig. S3, the percentages of $PU.1^+$ and $IRF8^+$ populations in PIB group reached 61.04% and 58.30%, respectively, which were significantly higher than those in the vPEM group (11.50% and 13.93%). These results demonstrated that the PIB-encoding plasmid had been successfully transfected into PEM.

It has been reported that PIB transcription factor combinations enable cells to acquire markers of DCs, along with retaining parental cell identity[10]. This strategy was regarded as partial reprogramming[10]. To characterize the phenotype of PIB-transfected PEM, the expression levels of DC markers ($CD11c^+$MHC-II^+) and macrophage markers ($F4/80^+$ and $CD11b^+$) were measured using flow cytometry in this study. As shown in Fig. 2C, the percentages of $CD11c^+$MHC-II^+ in PEM were 44.67%, 66.57%, and 69.73% on Days 5, 7, and 9 after PIB transfection, significantly higher than those in the vPEM group (15.50% on Day 9). These results suggested that a DC-like phenotype was successfully reprogrammed in PEM. Given the comparable percentages of $CD11c^+$MHC-II^+ on Days 7 and 9, PEM transfected with PIB-encoding plasmid for 7 days were used for subsequent experiments. As shown in Fig. 2D, the percentages of $F4/80^+$ (98.23%) and $CD11b^+$ (96.23%) in PIB group (PIB-transfected PEM) were similar to those in vPEM group on Day 7, suggesting that these cells preserved their original macrophage identity. Furthermore, the cell viability of PEMs was detected using the CCK-8 assay after transfection with the PIB-encoding plasmid for 7 days. As shown in Supporting Information Fig. S4, the PIB-transfected group exhibited high cell viability (>90%), with no significant difference compared to the vPEM group. This result indicated that the transfection procedure did not induce notable cytotoxicity in PEMs. Taken together, these results demonstrated that PIB-transfected PEM acquired a DC-like phenotype, along with preserving macrophage identity. These partially reprogrammed PEM were named DC-like M.

To evaluate the antigen presentation ability of DC-like M, these cells were pulsed with the MHC-I restricted epitope peptide ($OVA_{257-264}$) for 24 h. The expression levels of MHC-I and co-stimulatory molecules (CD80 and CD86) in DC-like M were measured using flow cytometry and RT-qPCR. As shown in Fig. 2E and F, the percentages of $CD80^+CD86^+$ (2.36-fold) population and SIINFEKL-H-$2Kb^+$ population (1.96-fold) in DC-like M group were significantly higher than those in vPEM group following treatment with $OVA_{257-264}$. Consistently, RT-qPCR results confirmed that DC-like M group significantly upregulated the expression of *CD86* and *H2KB* (*MHCI*) mRNA by 8.59- and 2.58-fold compared to vPEM group after treatment with $OVA_{257-264}$ (Supporting Information Fig. S5). These results indicated that DC-like M possessed enhanced antigen presentation ability through upregulation of MHC-I and co-stimulatory molecules.

To further improve the antigen presentation capability and the M1 phenotype polarization of DC-like M, these cells were stimulated with LPS (TLR4 agonist) and IFN-γ (pro-inflammatory cytokine) during $OVA_{257-264}$ pulsing. As reported, both LPS and IFN-γ could promote DC maturation and induce macrophage polarization towards M1 phenotype[29-31]. As shown in Fig. 2E and F, the percentages of $CD80^+CD86^+$ population (81.51%) and SIINFEKL-H-$2Kb^+$ population (77.38%) in DC-like M were significantly elevated after treatment with $OVA_{257-264}$, LPS, and IFN-γ, which were 2.43- and 1.75-fold higher than those cells treated with $OVA_{257-264}$ alone. Consistently, the mRNA expressions of *H2KB* and *CD86* in DC-like M were also upregulated by 1.33- and 2.40-fold following treatment with $OVA_{257-264}$, LPS, and IFN-γ, respectively (Fig. S5). Furthermore, as important markers of M1 phenotype macrophage, mRNA levels of *INOS* (374.33-fold) and *IL6* (161.42-fold) were significantly upregulated in DC-like M after treatment with $OVA_{257-264}$, LPS, and IFN-γ compared to those cells treated with $OVA_{257-264}$ alone (Supporting Information Fig. S6). These results demonstrated that the activated DC-like M1 macrophage (aDC-like M1) with dual functions of antigen presentation and M1 phenotype polarization was successfully constructed.

To evaluate the capability for activating $CD8^+$ T cells, the aDC-like M1 was co-cultured with $CD8^+$ T cells (isolated from OT-I mice) at a ratio of 1:3 for 72 h. These $CD8^+$ T cells isolated

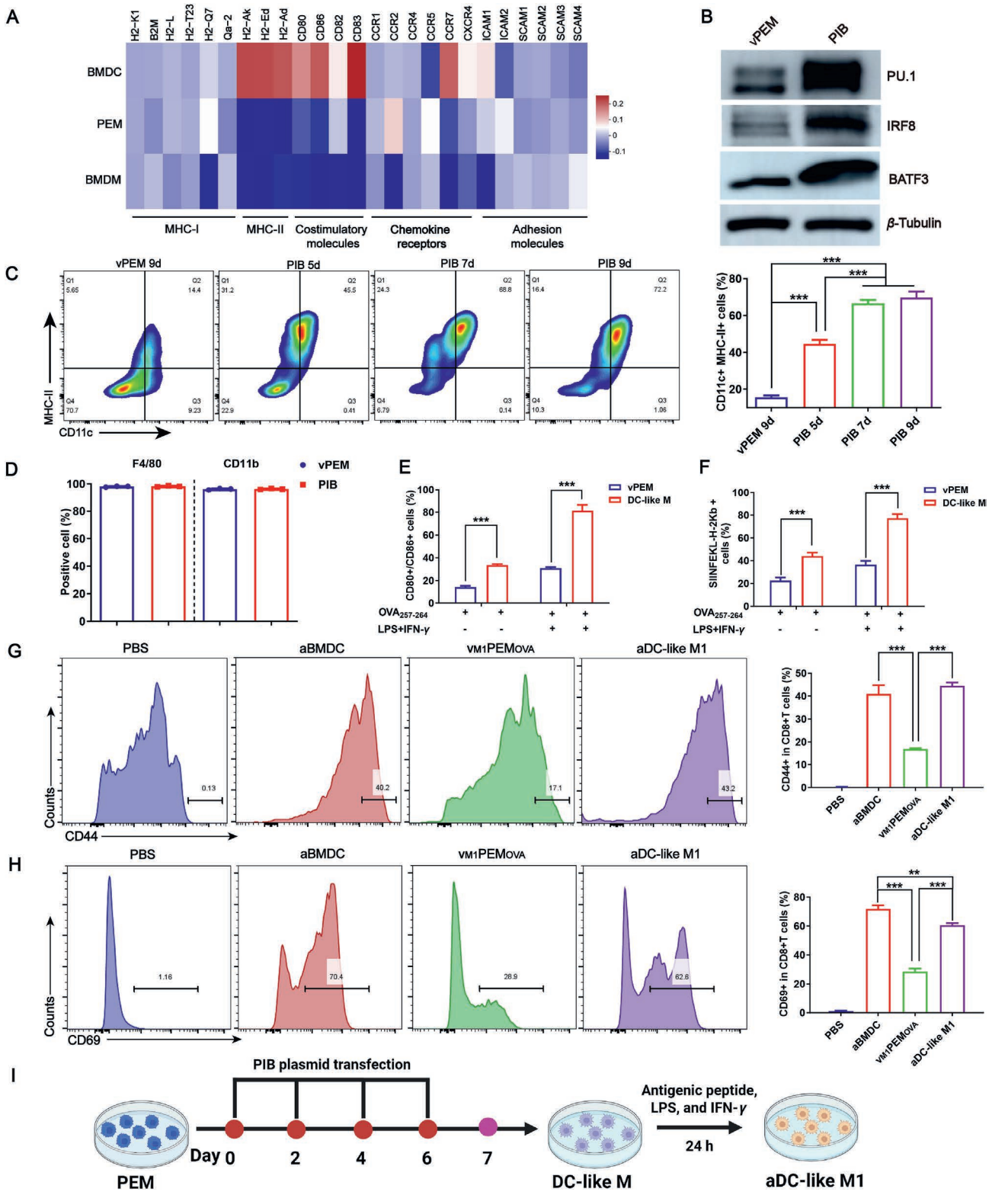

Figure 2 Reprogramming macrophages into activated DC-like M1 macrophages (aDC-like M1) based on the overexpression of transcription factor PIB. (A) Heatmap depicting expression of antigen presentation and migration-related proteins in bone marrow-derived dendritic cell (BMDC) and macrophage (BMDM), and peritoneal macrophage (PEM). (B) The expression levels of PU.1, IRF8, and BATF3 proteins in PEM after transfection with the PIB-encoding plasmid for 48 h vPEM: empty plasmid-transfected PEM. (C) Representative flow cytometry plots and the percentage of $CD11c^+$ $MHC\text{-}II^+$ population in PEM transfected with PIB-encoding plasmid for 5, 7, or 9 days. (D) The expression of macrophage markers (F4/80 and CD11b) in PEM after transfection with the PIB-encoding plasmid for 7 days. The percentage of (E) $CD80^+CD86^+$ population and (F) SIINFEKL-H-$2Kb^+$ population in DC-like M after treatment with LPS, IFN-γ, and $OVA_{257-264}$ for 24 h. The

from OT-I mice expressed a transgenic T cell receptor (TCR) that recognized $OVA_{257-264}$ in complex with the MHC-I molecule H-2Kb[32]. The aBMDC group (BMDC stimulated with LPS, IFN-γ, and $OVA_{257-264}$) and the $_{VM1}PEM_{OVA}$ group ($_{VM1}PEM_{OVA}$: PEM transfected with empty plasmid prior to stimulation with LPS, IFN-γ, and $OVA_{257-264}$) were set as control groups. The expression levels of activation markers of $CD8^+$ T cells (CD44 and CD69) were detected by flow cytometry. As shown in Fig. 2G and H, the aBMDC group exhibited significantly higher percentages of $CD44^+$ population (2.42-fold) and $CD69^+$ population (2.54-fold) in $CD8^+$ T cells than the $_{VM1}PEM_{OVA}$ group, indicating that superior $CD8^+$ T cell activation would be induced by BMDC. Notably, the aDC-like M1 group exhibited 2.63- and 2.12-fold higher percentages of $CD44^+$ population and $CD69^+$ population, respectively, among $CD8^+$ T cells, compared to the $_{VM1}PEM_{OVA}$ group. The percentage of $CD44^+CD8^+$ T cells in the aDC-like M1 group was similar to that in the aBMDC group, while the percentage of $CD69^+CD8^+$ T cells was slightly lower. These results revealed that aDC-like M1 possessed an excellent capability to activate $CD8^+$ T cells, which was likely due to the elevated expression of peptide-MHC-I complexes (pMHC-I) and co-stimulatory molecules (Fig. 2E and F).

The above results demonstrated that reprogramming PEM towards an aDC-like M1 phenotype successfully occurred as a stepwise process through PIB transfection followed by treatment with antigenic peptide ($OVA_{257-264}$), LPS, and IFN-γ (Fig. 2I). These aDC-like M1 exhibited dual functions of antigen presentation and M1 phenotype polarization, which could be sufficient to elicit $CD8^+$ T cell activation and remodel TME. Although further refinement of the DC reprogramming strategy might strengthen DC identity, partial reprogramming facilitated the retention of pro-inflammatory mediators in M1 macrophages and supported TME remodeling and T cell activation against cold tumors. This highlighted the advantage of utilizing macrophage reprogramming for tumor immunotherapy.

3.2. Preparation and characterization of MAC-PNV

Nanovesicles (NVs), inheriting bioactive components and functional properties from their parent cells, have emerged as promising immunotherapeutic agents[15,33-35]. As reported, NVs produced by methods such as mechanical extrusion, freeze-thaw cycling, and ultrasonication have been regarded as effective alternatives to natural extracellular vesicles (EVs)[33,36]. NVs exhibited similar physicochemical characteristics and biological functions to EVs, but their yield was 20−100 times greater than that of EVs, rendering them highly suitable for scalable production and future clinical translation[33,36]. Building on these advantages, aDC-like M1-derived nanovesicles (MAC-PNV) were prepared *via* sequential extrusion and gradient centrifugation in this study (Fig. 3A). As shown in Fig. 3B and C, MAC-PNV exhibited a uniform average particle size of 177.3 nm, a narrow size distribution (PDI of 0.21), and a zeta potential of −20.8 mV, measured using dynamic light scattering (DLS). Transmission electron microscopy (TEM) further revealed that MAC-PNV exhibited a typical cup-shaped morphology (Fig. 3D), consistent with structural features of M1 macrophage-derived NVs reported in previous literature[15]. In addition, the yield of MAC-PNV was quantified by measuring the total protein content of MAC-PNV derived from a defined number of parent cells. The results showed that 2.45 ± 0.14 mg of total proteins could be obtained from 1×10^8 aDC-like M1. Furthermore, the protein recovery rate for MAC-PNV was approximately 25.6%. The NVs derived from aBMDC (DC-NV) or $_{VM1}PEM_{OVA}$ (MAC-CNV) were prepared as control groups, which exhibited physicochemical properties similar to MAC-PNV, including size, zeta potential, and TEM morphology (Supporting Information Fig. S7). The results of the storage stability assay demonstrated that MAC-PNV maintained a stable particle size (∼180 nm) within 5 days at 4 °C (Fig. 3E). Furthermore, no significant changes in particle size (∼180 nm) and total protein contents (∼1.4 mg/mL) were found in MAC-PNV after 1 month of cryopreservation at −80 °C (Fig. 3F), indicating robust stability under long-term storage conditions. Additionally, Western blotting confirmed that MAC-PNV presented classic EVs markers, including CD9, CD81, TSG101, and Alix (Fig. 3G).

To investigate the potential of MAC-PNV to activate $CD8^+$ T cells, the levels of antigen-presenting molecules (MHC-I) and co-stimulatory molecules (CD80, CD86, CD83, and CD40) in MAC-PNV were measured using LC/MS−MS and Western blotting assays. Significantly higher levels of MHC-I, CD80, CD86, CD83, and CD40 were shown in MAC-PNV than those in MAC-CNV (Fig. 3H). Consistently, Western blotting images further demonstrated the significant upregulation of key antigen presentation components (MHC-I, CD80, and CD86) in MAC-PNV compared to MAC-CNV (Fig. 3I). Given the critical roles of antigen-presenting molecules and co-stimulatory molecules in initiating $CD8^+$ T immune responses, these results suggested that MAC-PNV possessed excellent potential to activate $CD8^+$ T cells. In addition, compared to DC-NV, MAC-PNV exhibited comparable levels of MHC-I, CD86, and CD83, while slightly lower levels of CD80 and CD40 (Fig. 3H and I). These results might result from the limited partial reprogramming effects of PIB transfection on DC-like M. Furthermore, three independent batches of MAC-PNV exhibited consistent levels in MHC-I, CD80, and CD86 proteins, indicating robust inter-batch reproducibility of the preparation protocol (Fig. 3J).

Collectively, these results revealed that MAC-PNV exhibited robust physicochemical properties (size, charge), good stability, batch-to-batch reproducibility, and abundant antigen-presenting-related components (*e.g.*, MHC-I, CD80, and CD86), which were essential requirements for both *in vitro* and *in vivo* applications.

3.3. Enhanced functions of $CD8^+$ T cells activated by MAC-PNV in vitro

The activation of antigen-specific $CD8^+$ T cells requires two critical signals[28]. The first signal provided by T cell receptors (TCR) recognition of pMHC-I is to specifically initiate $CD8^+$ T cell activation. The second signal mediated by the interaction of co-stimulatory molecules CD80/CD86 with CD28 is to promote $CD8^+$ T cell proliferation and effector functions[28]. These two signals ensure the effective activation of $CD8^+$ T cells that enable them to proliferate and differentiate[28,37].

percentages of (G) $CD44^+$ population and (H) $CD69^+$ population among $CD8^+$ T cells after co-culture of different cells with OT-I mouse-derived $CD8^+$ T cells at a 1:3 ratio for 72 h. (I) Schematic illustration of the preparation process of aDC-like M1. Created with BioRender (https://biorender.com/). Data are represented as mean ± SD ($n = 3$). *$P < 0.05$, **$P < 0.01$, ***$P < 0.001$.

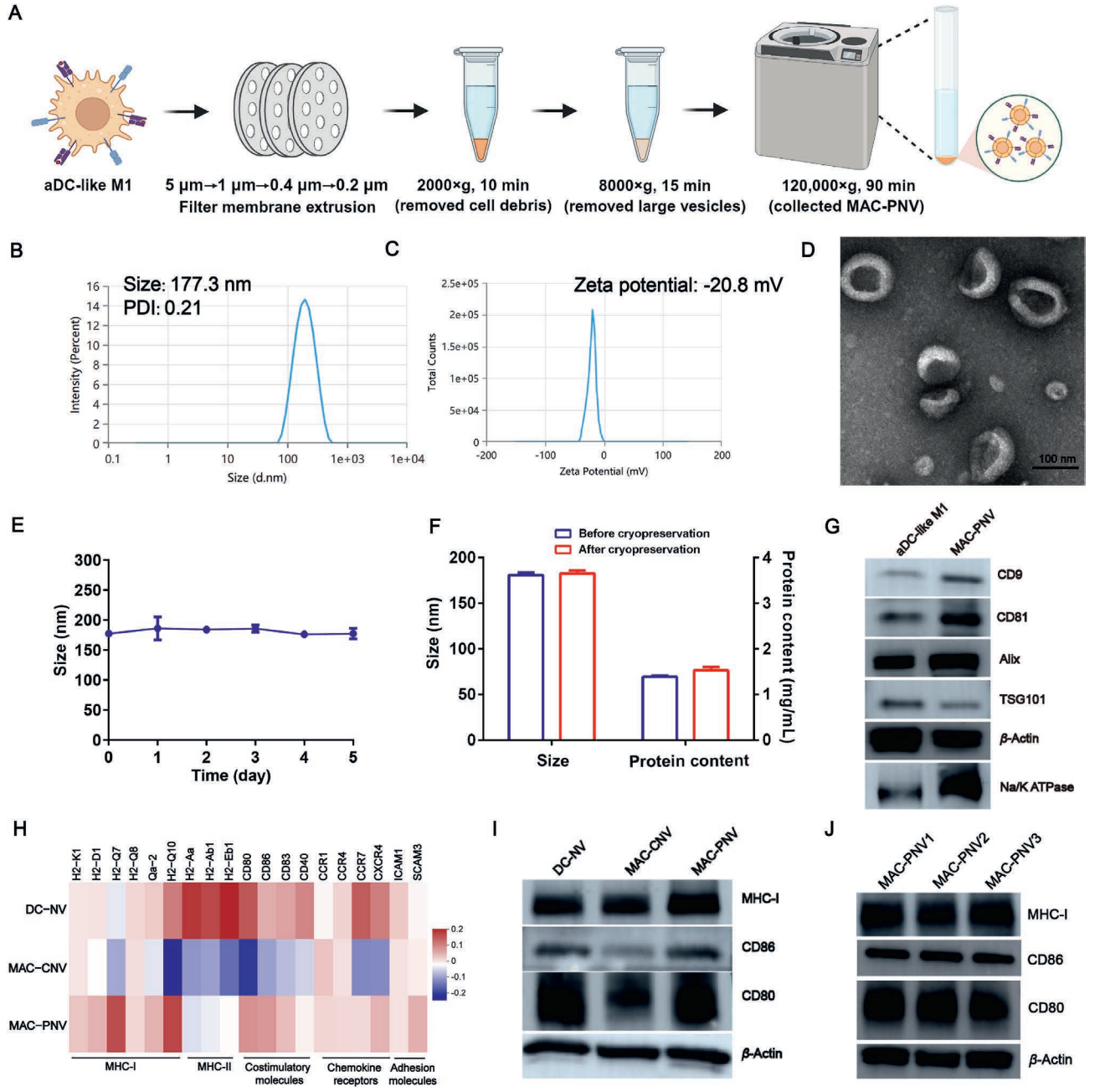

Figure 3 Characterization of MAC-PNV. (A) Schematic illustration of MAC-PNV preparation. Created with BioRender (https://biorender.com/). (B) Mean particle size, polydispersity index (PDI), and (C) zeta potential of MAC-PNV detected using DLS. (D) TEM images of MAC-PNV. Scale bar = 100 nm. (E) The size changes of MAC-PNV within 5 days when stored at 4 °C. (F) The size and protein content of MAC-PNV before and after cryopreservation at −80 °C for 1 month. (G) The contents of CD9, CD81, Alix, and TSG101 proteins in MAC-PNV detected using Western blotting. (H) Heatmap depicting expression of antigen presentation and migration-related proteins in DC-NV, MAC-CNV, and MAC-PNV detected using LC−MS/MS. (I) The levels of CD80, CD86, and MHC-I protein in MAC-PNV. (J) The levels of CD80, CD86, and MHC-I protein in three independent batches of MAC-PNV.

Considering that it has higher levels of MHC-I and co-stimulatory molecules (*e.g.*, CD80/CD86), we hypothesized that MAC-PNV containing two signals might directly activate naïve $CD8^+$ T cells through the interaction of pMHC-I−TCR and CD80/86−CD28. To assess whether the activation and proliferation of antigen-specific $CD8^+$ T cells were induced by MAC-PNV, the OVA-specific $CD8^+$ T cells (isolated from OT-I mice) were co-cultured with MAC-PNV for 72 h (Fig. 4A). The levels of markers (CD44 and CD69) and the proliferation rate of activated $CD8^+$ T cells were detected by flow cytometry and cell counter. As shown in Fig. 4B and C, the percentages of $CD44^+$ $CD8^+$ T population (35.20%) and $CD69^+$ $CD8^+$ T population (62.77%) in the $CD8^+$ T cells treated with MAC-PNV were significantly higher than those treated with MAC-CNV (11.83% and 28.27%, respectively), indicating that MAC-PNV had stronger effects on promoting $CD8^+$ T cell activation. The highest percentage of

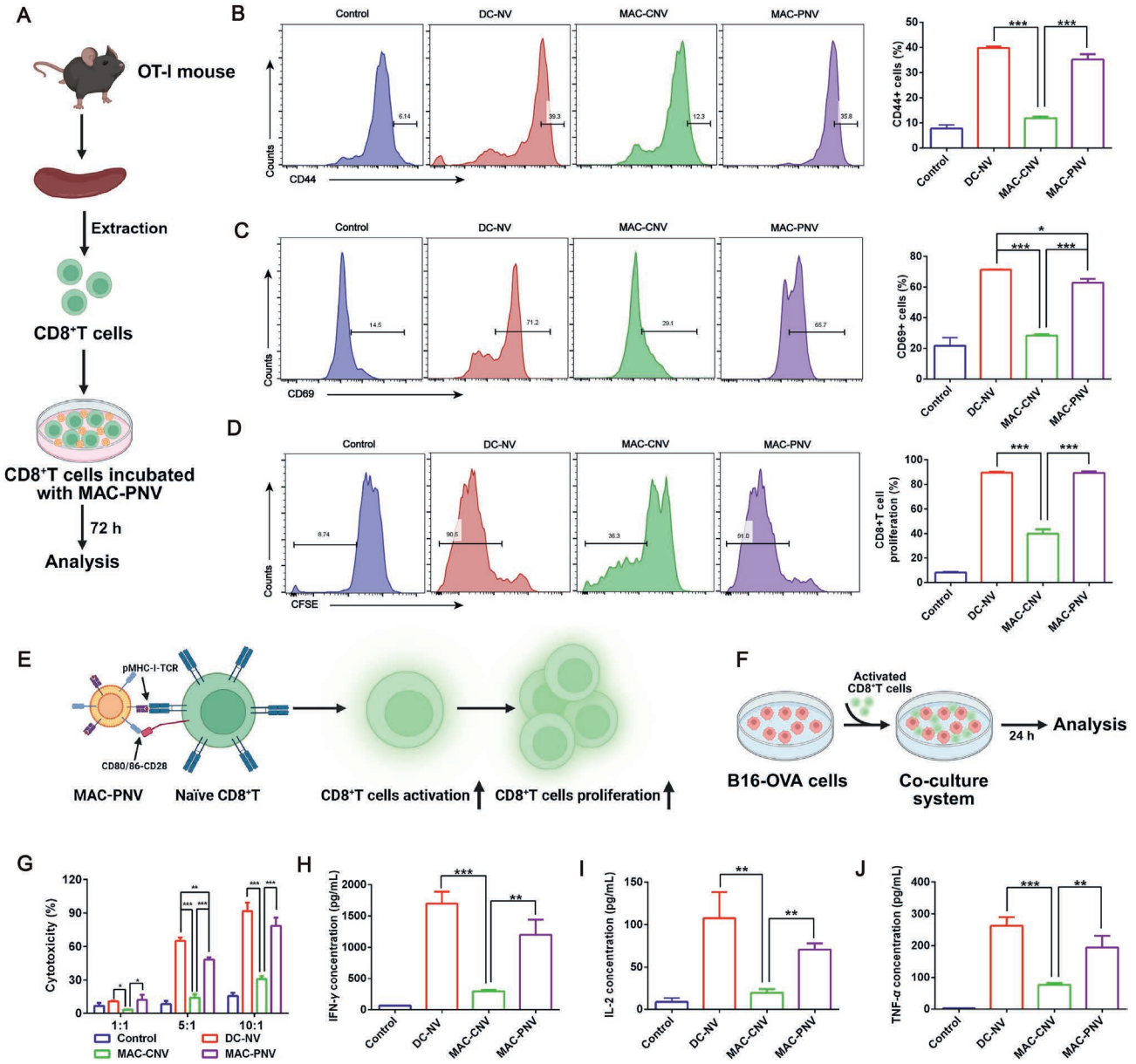

Figure 4 Enhanced functions of CD8$^+$ T cells activated by MAC-PNV *in vitro*. (A) Schematic illustration of the experimental design. The OVA-specific CD8$^+$ T cells (isolated from OT-I mice) were co-cultured with MAC-PNV for 72 h to analyze the activation and proliferation of CD8$^+$ T cells. Created with BioRender (https://biorender.com/). The percentages of (B) CD44$^+$ population and (C) CD69$^+$ population in CD8$^+$ T cells detected by flow cytometry. (D) Proliferation rate of CD8$^+$ T cells measured using flow cytometry. (E) Schematic illustration of MAC-PNV-induced activation and proliferation of CD8$^+$ T cells. (F) Schematic illustration of the experimental design. B16-OVA cells were co-cultured with activated CD8$^+$ T cells at various effector/target (E:T) ratios for 24 h. Created with BioRender (https://biorender.com/). (G) The killing efficiency of CD8$^+$ T cells against B16-OVA cells at various effector/target (E:T) ratios detected by the lactate dehydrogenase (LDH) assay kit. The levels of (H) IFN-γ, (I) IL-2, and (J) TNF-α in the supernatants of CD8$^+$ T cells detected using ELISA kits. Data are represented as mean ± SD ($n = 3$). $^*P < 0.05$, $^{**}P < 0.01$, $^{***}P < 0.001$.

CD69$^+$ CD8$^+$ T population (71.23%) in the CD8$^+$ T cells was shown in DC-NV group, which might result from the highest levels of co-stimulatory molecules (CD80 and CD40) in DC-NV (Fig. 4C). Furthermore, equivalent to DC-NV group, MAC-PNV group exhibited 2.23-fold higher proliferation rate of CD8$^+$ T cells than MAC-CNV group (Fig. 4D). In addition, the result of the cell counting assay showed that the number of CD8$^+$ T cells in MAC-PNV group was 2.42-fold higher than that in MAC-CNV group (Supporting Information Fig. S8). These results demonstrated that the potent activation and proliferation of CD8$^+$ T cells were successfully induced by MAC-PNV contained MHC-I and co-stimulatory molecules (*e.g.*, CD80/CD86) (Fig. 4E).

To evaluate the tumor-killing capability of CD8$^+$ T cells activated by MAC-PNV, B16-OVA cells were co-cultured with activated CD8$^+$ T cells at various effector/target (E:T) ratios for 24 h (Fig. 4F). The killing efficiency of activated CD8$^+$ T cells was evaluated by the level of LDH released from B16-OVA cells, which was measured by the LDH kit. The viability of B16-OVA

cells was detected by MTT assay. As shown in Fig. 4G, the cytotoxicity results demonstrated that significantly stronger killing efficiency of $CD8^+$ T cells against B16-OVA cells was found in MAC-PNV group than that in MAC-CNV group at various E:T ratios. At the E:T ratio of 10:1, the killing efficiency of $CD8^+$ T cells in the MAC-PNV group was 2.53-fold higher than that in the MAC-CNV group and even comparable to that in DC-NV group. Moreover, as shown in the results of the MTT assay (Supporting Information Fig. S9), significantly lower viabilities of B16-OVA cells were found in MAC-PNV and DC-NV groups than those in MAC-CNV group. These results demonstrated that $CD8^+$ T cells activated by MAC-PNV could efficiently kill tumor cells.

As reported, IFN-γ and TNF-α produced by activated $CD8^+$ T cells directly induce tumor cell apoptosis[38], and IL-2 drives the $CD8^+$ T cell expansion and differentiation[39], endowing $CD8^+$ T cells with superior anti-tumor properties. To investigate the cytotoxicity mechanism of $CD8^+$ T cells mediated by MAC-PNV, the levels of IFN-γ, TNF-α, and IL-2 secreted by activated $CD8^+$ T cells were measured using ELISA kits. Compared to MAC-CNV group, MAC-PNV group exhibited significantly higher levels of three inflammatory cytokines, including IFN-γ (4.07-fold), TNF-α (2.55-fold), and IL-2 (3.61-fold) (Fig. 4H–J).

In summary, the above results demonstrated that MAC-PNV could significantly promote activation and proliferation of antigen-specific $CD8^+$ T cells, thereby enabling them to enhance killing effects on tumor cells through secretion of effector molecules (*e.g.*, IFN-γ and TNF-α).

3.4. Enhanced macrophage repolarization induced by MAC-PNV in vitro

The immune evasion and resistance in tumor therapy are usually related to immunosuppressive TME[40]. As a predominant immune-related cell population in the TME, M2 TAMs often drive immunosuppression *via* secreting cytokines (*e.g.*, IL-10, TGF-β), expressing immune checkpoint molecules (*e.g.*, PD-L1), and recruiting regulatory T cells (Tregs), thereby limiting the efficiency of tumor immunotherapy[41,42]. It has been reported that the M1 macrophage-derived NVs or exosomes could effectively improve anti-tumor effects by remodeling TME with the change of M2 TAMs towards M1 phenotype[15]. Considering that the identity of macrophages was retained in aDC-like M1, we hypothesized that the MAC-PNV would obtain the repolarization capability on M2 TAMs.

To verify whether MAC-PNV could induce the repolarization of macrophages from M2 to M1 phenotype, the M2 macrophage model was established from PEM stimulated by IL-4 (Fig. 5A). As shown in Fig. 5B–E, significantly higher percentages of $CD206^+$ population and lower percentages of $CD86^+$ population were found in macrophages treated with IL-4 (IL-4 group) than those in untreated (Control group), suggesting that M2 macrophages were successfully established *via* IL-4 stimulation. These established M2 macrophages were treated with DC-NV, MAC-CNV, and MAC-PNV, respectively. After being treated for 24 h, the levels of phenotypic markers (CD86, IL-12, and IL-6 for M1; CD206 and Arg-1 for M2) in macrophages were detected by flow cytometry and RT-qPCR. As shown in Fig. 5C–E, the lowest percentages of $CD206^+$ population (4.61%) and the highest percentages of $CD86^+$ population (33.83%) were found in macrophages treated with MAC-PNV, and the lowest M2/M1 polarization index (ratio of $CD206^+/CD86^+$ cells = 0.14) was observed in MAC-PNV among the three groups, suggesting that MAC-PNV showed the best repolarization effects. Compared to DC-NV group, MAC-CNV group showed better repolarization effects, evidenced by 41.78% reduction in the percentage of $CD206^+$ population and 1.44-fold increase in the percentage of $CD86^+$ population in macrophages (Fig. 5D and E). In addition, RT-qPCR results further demonstrated that MAC-PNV group exhibited stronger downregulatory effects on the mRNA levels of *CD206* (77.65%) and *ARG1* (87.40%) than DC-NV group (50.09% and 66.49%, respectively) and MAC-CNV (61.28% and 66.02%, respectively) groups (Fig. 5F and G). Meanwhile, MAC-PNV group markedly upregulated the levels of *IL6* and *IL12* mRNA, compared to the DC-NV group (by 6.40- and 3.88-fold, respectively), and MAC-CNV group (by 1.29- and 1.61-fold, respectively) (Fig. 5H and I). These results demonstrated that MAC-PNV exhibited the strongest repolarization effects on M2 macrophages toward the M1 phenotype.

It has been reported that M1 macrophages could promote the activation of $CD8^+$ T cells and induce tumor cell apoptosis by secreting inflammatory mediators such as TNF-α, IFN-γ, and NO[43,44]. Additionally, M1 macrophages could recruit $CD8^+$ T cells by secreting CXCL9 and CXCL10[45]. To evaluate whether MAC-PNV-induced repolarization of M2 macrophages resulted in the secretion of these key mediators, the levels of TNF-α, IFN-γ, NO, and CXCL10 were quantified using ELISA kits and NO assay. As shown in Fig. 5J–M, MAC-PNV group exhibited significantly higher levels of TNF-α, IFN-γ, NO, and CXCL10, compared to the DC-NV group (4.55-, 2.31-, 2.29-, and 2.35-fold, respectively), and MAC-CNV group (1.35-, 1.52-, 1.34-, and 1.40-fold, respectively). These results indicated that M2 macrophages repolarized by MAC-PNV treatment could significantly enhance the secretion of TNF-α, IFN-γ, NO, and CXCL10.

The cargo in MAC-PNV is pivotal for its repolarization effects on M2 macrophages. As reported, miR-125a-5p, miR-125b-5p, miR-132-3p, *TNFA* mRNA, and *INOS* mRNA drive macrophage polarization towards the M1 phenotype, while let-7c-5p, miR-9, and miR-146b-5p favor macrophage polarization towards the M2 phenotype[15,46-49]. To elucidate the mechanism of M2 macrophage repolarization mediated by MAC-PNV, the levels of miRNAs (miR-125a-5p, miR-125b-5p, miR-132-3p, let-7c-5p, miR-9, and miR-146b-5p) and mRNAs (*TNFA* and *INOS*) related to macrophage polarization in MAC-PNV were detected by RT-qPCR. As shown in Fig. 5N, significantly higher levels of pro-M1 polarization mediators (miR-125a-5p, miR-125b-5p, miR-132-3p, *TNFA* mRNA, and *INOS* mRNA) were observed in MAC-PNV than those in MAC-CNV and DC-NV, and significantly lower levels of pro-M2 polarization mediators (let-7c-5p, miR-9, and miR-146b-5p) were found in MAC-PNV than those in DC-NV, suggesting that MAC-PNV obtained stronger repolarization effects on M2 macrophages toward M1 phenotype. It has been reported that PU.1 and IRF8 were pro-M1 macrophage polarization transcription factors that induced downstream M1-specific gene expressions[50-52]. We thought that the stronger repolarization effects of MAC-PNV might be attributed to the overexpression of PU.1 and IRF8 in their parental cells (aDC-like M1).

To further verify the macrophages repolarization effects, the cargo of MAC-PNV was eliminated through the treatment of saponin (Saponin-treated MAC-PNV group)[24]. As shown in Supporting Information Fig. S10A–S10C, after treatment with saponin, 95.40% of RNA and 57.29% of protein were eliminated from MAC-PNV, and MAC-PNV still maintained its nanoscale size ($\sim$190 nm). The repolarization effects of saponin-treated MAC-PNV were evaluated by detecting the levels of CD206

and CD86 in macrophages using flow cytometry. The results revealed that a substantial increase in the percentage of $CD206^+$ population (from 4.65% to 19.26%) and a marked decrease in the percentage of $CD86^+$ population (from 24.60% to 6.89%) in macrophages were found in Saponin-treated MAC-PNV group, compared to MAC-PNV group, indicating that the repolarization capability of MAC-PNV was inhibited by the elimination of cargo (Fig. S10D−S10G).

To further investigate the functional properties of macrophages repolarized by MAC-PNV, their phagocytic activity and capacity to activate $CD8^+$ T cells were assessed. The IL-4-stimulated M2 macrophages were treated with MAC-PNV for 24 h and then co-incubated with CFSE-labeled B16-F10 tumor cells for 12 h. Phagocytic activity of these macrophages was determined by flow cytometry as the percentage of $CFSE^+CD11b^+$ population. As shown in Fig. 5O, the highest percentage of $CFSE^+CD11b^+$ population was found in the MAC-PNV (12.80%) group, representing a 1.74- and 3.23-fold higher than that in the MAC-CNV and DC-NV groups, respectively. These results indicated that M2 macrophages repolarized to the M1 phenotype by MAC-PNV acquired the strongest phagocytic activity against B16-F10 cells. Furthermore, to evaluate the capacity of repolarized macrophages to activate $CD8^+$ T cells, M2 macrophages were pulsed with $OVA_{257-264}$ peptide after treatment with MAC-PNV for 24 h. Then, these macrophages were co-cultured with CFSE-labeled OT-I $CD8^+$ T cells for 72 h. As shown in Fig. 5P, the proliferation rate of $CD8^+$ T cells in the MAC-PNV group (28.50%) was significantly higher than that in the MAC-CNV (22.20%) and DC-NV (4.15%) groups. Taken together, these results demonstrated that MAC-PNV-repolarized macrophages acquired enhanced anti-tumor functions, including potent phagocytic activity and the capacity to activate $CD8^+$ T cells.

Collectively, these results demonstrated that MAC-PNV possessed the most potent capability to repolarize pro-tumor M2 macrophages towards an anti-tumor M1 phenotype, primarily mediated by its enriched cargo of pro-M1 polarization mediators (*e.g.*, *TNFA*/*iNOS* mRNAs and miR-125/132 clusters) (Fig. 5Q). These changes resulted in enhanced phagocytic activity and a superior capacity for $CD8^+$ T cell activation by the repolarized macrophages, highlighting the significant therapeutic potential of MAC-PNV.

3.5. *In vivo therapeutic efficacy of MAC-PNV alone*

To evaluate the anti-tumor efficacy of MAC-PNV, primary B16-OVA tumor-bearing C57BL/6J mice were divided into four groups, including PBS, DC-NV, MAC-CNV, and MAC-PNV groups. PBS solution and various NVs (1 mg/mL of total protein, 100 μL per mouse) were injected peritumorally every 3 days (Fig. 6A). The tumor volume and body weight of the mice were monitored and recorded every 2 days. On the 11th day after treatment, the mice were euthanized, and the weight of the excised tumor tissues and the immune-related indicators were measured. As shown in Fig. 6B, the strongest tumor growth inhibition (77.00%) was found in the mice treated with MAC-PNV, significantly higher than that of the DC-NV group (45.19%) and the MAC-CNV group (48.74%). Additionally, the MAC-PNV group exhibited the strongest tumor weight inhibition rate (79.03%) (Fig. 6C). Furthermore, as seen from the survival curve (Fig. 6D), the median survival period of mice was significantly prolonged in MAC-PNV group (33 days), compared to the PBS group (21 days), DC-NV group (25 days), and MAC-CNV group (27 days). No significant change in body weight was observed during the whole treatment (Fig. 6E). Hematoxylin and eosin (H&E) staining images showed that no pathological abnormality was seen in the heart, liver, spleen, lung, and kidney of mice after various treatments (Supporting Information Fig. S11). Collectively, these results demonstrated that MAC-PNV treatment significantly suppressed tumor growth, prolonged survival, and exhibited good biosafety in the B16-OVA melanoma mouse model.

To elucidate the *in vivo* anti-tumor immune response of MAC-PNV, the percentage of $CD8^+$ T cells in TDLNs and the number of tumor-infiltrating $CD8^+$ T cells were evaluated using flow cytometry and immunofluorescence analysis. The results of *ex vivo* imaging revealed that all Cy7-labeled NVs efficiently accumulated in TDLNs at 48 h after peritumoral injection, which might facilitate activating TDLN-resident $CD8^+$ T cells (Supporting Information Fig. S12D and S12E). As shown in Fig. 6F, MAC-PNV group (43.14%) exhibited the highest percentage of $CD8^+$ T cells (gated on $CD45^+CD3^+$) in TDLNs, compared to MAC-CNV (36.07%) and DC-NV (40.10%) groups. Since the activated $CD8^+$ T cells might migrate into tumors to exert cytotoxic effects, the intra-tumoral $CD8^+$ T cell infiltration was assessed. Immunofluorescence staining images revealed markedly increased counts of tumor-infiltrating $CD8^+$ T cells (red fluorescent dots) in MAC-PNV group compared to MAC-CNV and DC-NV groups (Fig. 6G). Furthermore, the significantly elevated percentage of IFN-γ^+CD8^+ T cells (gated on $CD45^+$ $CD3^+$) in tumors was observed in the MAC-PNV group, exhibiting 2.35- and 1.56-fold increases compared to MAC-CNV and DC-NV groups, respectively (Fig. 6H). The improved intra-tumoral infiltration of $CD8^+$ T cells might be attributed to the increased counts of activated $CD8^+$ T cells and the enhanced TME remodeling effects mediated by MAC-PNV. These data demonstrated that MAC-PNV treatment initiated $CD8^+$ T cell activation in TDLNs and enhanced intra-tumoral infiltration of activated $CD8^+$ T cells, especially IFN-γ^+CD8^+ T cells.

In addition to $CD8^+$ T cell activation, the capability of MAC-PNV for TME remodeling was also investigated. The results of *in vivo* imaging showed that strong fluorescence intensities of MAC-CNV and MAC-PNV groups were observed in tumor tissues and remained for up to 48 h after peritumoral injection, while the fluorescence signals of DC-NV group almost disappeared at 48 h (Fig. S12A−S12C). The prolonged retention of MAC-CNV and MAC-PNV in tumor tissues might be attributed to tumor-homing capability inherited from macrophages, which might benefit TME remodeling[15,53]. Then, the ratio of M1/M2 TAMs, the percentage of Tregs, and the levels of proinflammatory cytokines within tumors were assessed using flow cytometry, immunofluorescence, and ELISA analysis, respectively. As shown in Fig. 6I, immunofluorescence staining images confirmed the fewest counts of M2 TAMs (red signal) in MAC-PNV group compared to all other groups. Moreover, MAC-PNV group exhibited the highest M1/M2 TAMs ratio (0.77) (gated on $CD11b^+F4/80^+$) compared to DC-NV group (0.40) and MAC-CNV group (0.56) (Fig. 6J). These results indicated that MAC-PNV treatment induced the strongest repolarization effects on M2 TAMs towards the M1 phenotype. In addition, as a key immunosuppressive T cell subset mainly recruited by M2 TAMs[54], the percentage of Tregs ($CD25^+FoxP3^+$ populations gated on $CD45^+CD3^+$) was quantified in tumor tissues. As shown in Fig. 6K, a significantly lower percentage of Tregs was observed in MAC-PNV (12.29%) group than that in DC-NV (18.29%) and MAC-CNV (20.29%) groups, which was attributed to the stronger repolarization effects of MAC-PNV on

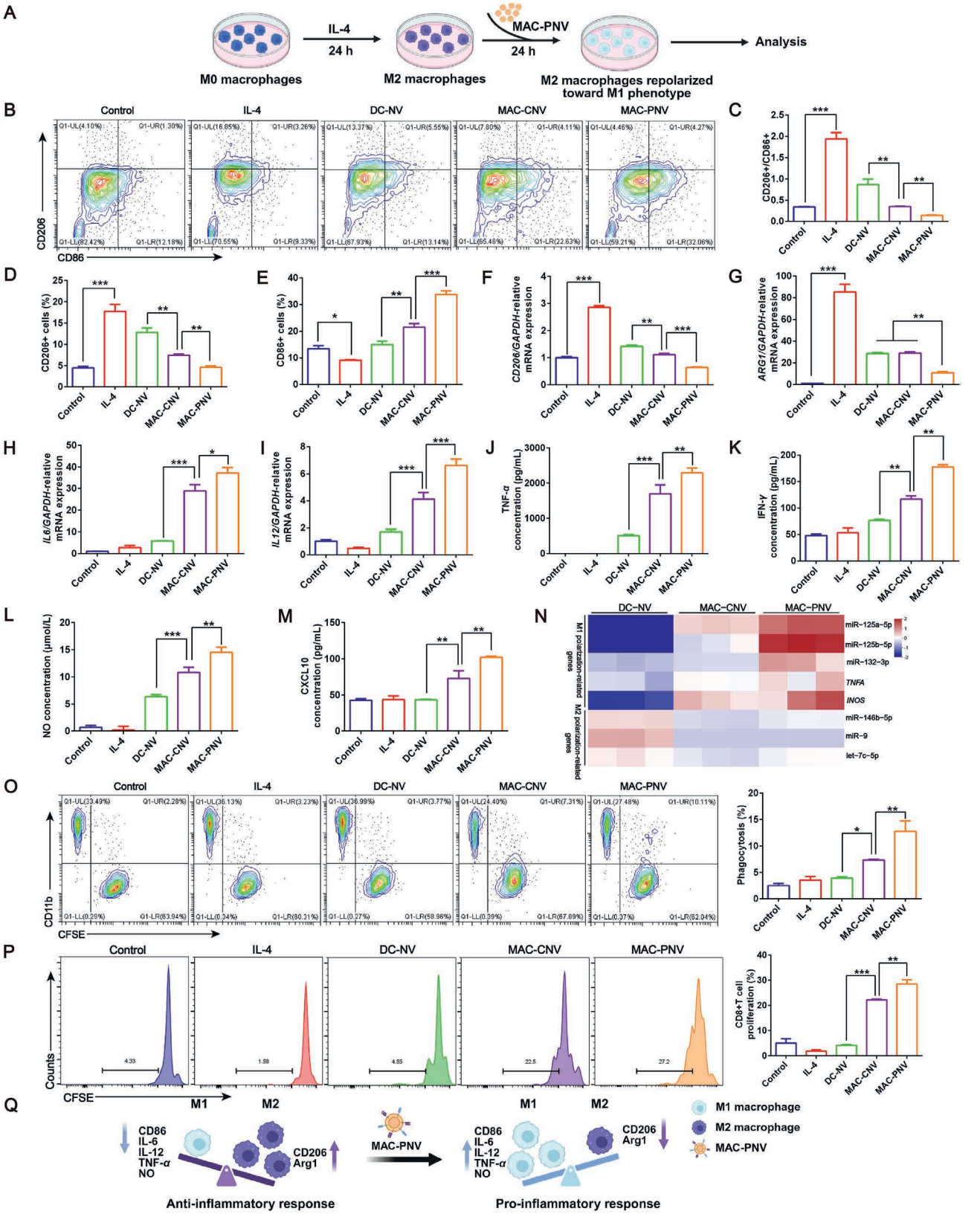

Figure 5 Enhanced macrophage repolarization induced by MAC-PNV in IL-4-induced M2 macrophages. IL-4 group referred to the IL-4-stimulated PEM with an M2 phenotype. Control group referred to the PEM without IL-4 treatment. (A) Schematic illustration of the experimental design. PEMs (M0 phenotype) were polarized into the M2 phenotype after being stimulated with IL-4 for 24 h. These M2 macrophages were then co-cultured with MAC-PNV for 24 h to achieve repolarization. Created with BioRender (https://biorender.com/). (B) Representative flow cytometry plots of CD206 and CD86-positive populations after incubating M2 macrophages with different NVs for 24 h. (C) M2/M1

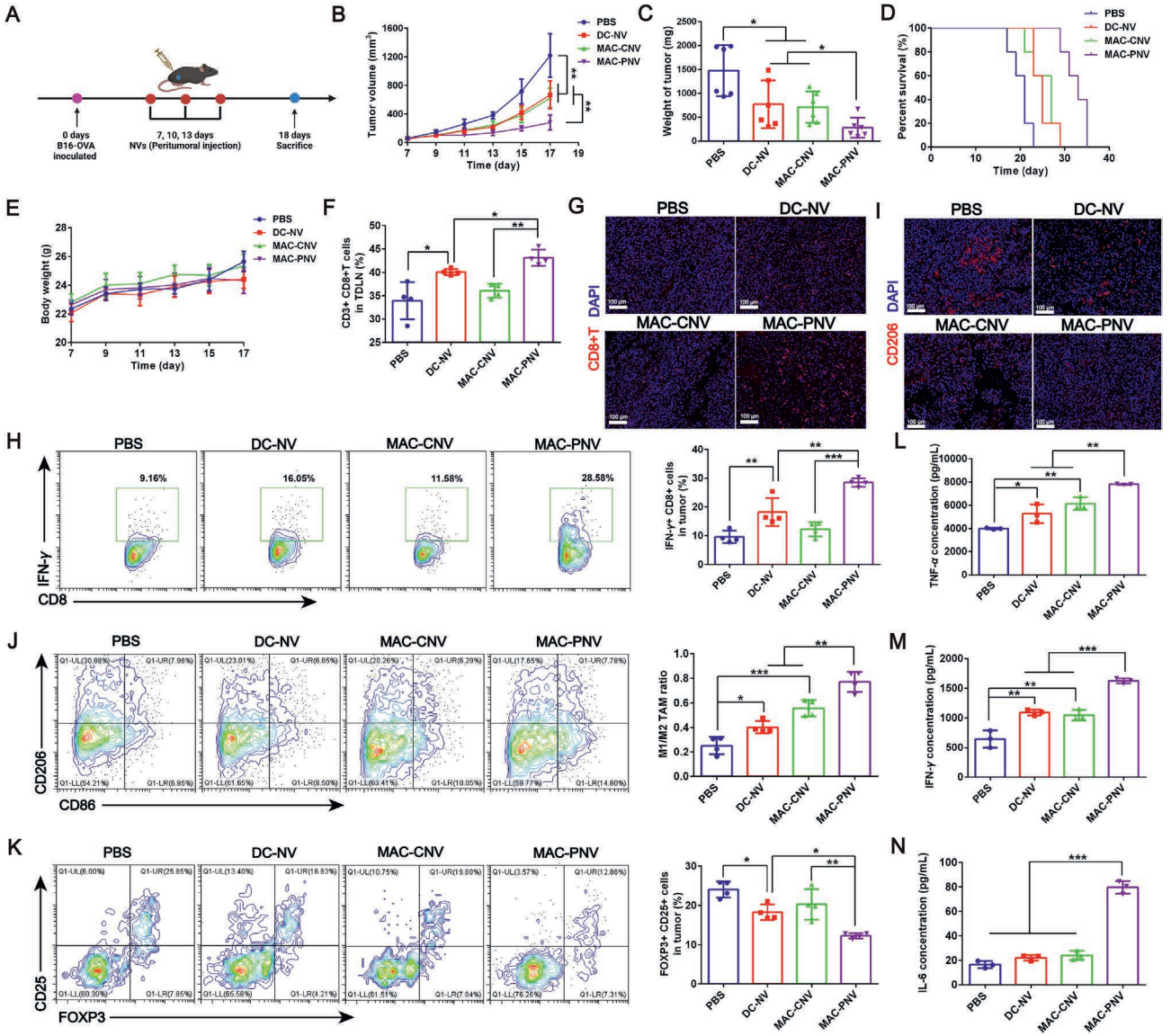

Figure 6 *In vivo* anti-tumor efficacy and immune responses of MAC-PNV in B16-OVA tumor-bearing C57BL/6J mice. (A) Schematic illustration of the experimental design. The B16-OVA-bearing mice were injected peritumorally with different NVs on the 7th, 10th, and 13th days, respectively. (B) Tumor growth curves of mice treated with different NVs ($n = 6$). (C) Tumor weights of mice treated with different NVs on the 18th day ($n = 6$). (D) The survival rate of mice after treatment with different NVs ($n = 5$). (E) The body weight of mice during the experiment after different treatments ($n = 6$). (F) The percentage of $CD8^+$ T cells (gated on $CD3^+$ $CD45^+$) in TDLNs ($n = 4$). (G) Representative immunofluorescence staining images of $CD8^+$ T cells (red) in tumors. The nucleus was stained with DAPI (blue). Scale bars, 100 μm. (H) Representative flow cytometry plots and the percentage of IFN-γ^+CD8^+ T cells (gated on $CD3^+$ $CD45^+$) in tumor tissues ($n = 4$). (I) Representative immunofluorescence staining images of $CD206^+$ macrophages (red) in tumors. The nucleus was stained with DAPI (blue). Scale bars, 100 μm. (J) Representative flow cytometry plots of M2 and M1 TAM (gated on $F4/80^+CD11b^+$) and the ratio of M1/M2 TAMs ($n = 4$). (K) Representative flow cytometry plots and the percentage of Tregs (gated on $CD3^+$ $CD45^+$) in tumor tissues ($n = 4$). The levels of (L) TNF-α, (M) IFN-γ, and (N) IL-6 in tumors after different treatments ($n = 3$). Data are represented as mean ± SD. $^*P < 0.05$, $^{**}P < 0.01$, $^{***}P < 0.001$.

polarization index ($CD206^+/CD86^+$ ratio) detected using flow cytometry. The percentage of (D) CD206-positive and (E) CD86-positive populations. The relative mRNA expression levels of (F) *CD206* and (G) *ARG1* (M2 macrophage marker) quantified using RT-qPCR after incubating M2 macrophages with different NVs for 24 h. The relative mRNA expression levels of (H) *IL6* and (I) *IL12* (M1 macrophage marker) quantified using RT-qPCR. The expression levels of (J) TNF-α, (K) IFN-γ, (L) NO, and (M) CXCL10 quantified using ELISA kits and the NO assay. (N) Heatmap depicting expression of polarization-regulating miRNAs/mRNAs in NVs quantified using RT-qPCR. (O) Phagocytic activity of macrophages against B16-F10 cells determined by flow cytometry. (P) Proliferation rate of $CD8^+$ T cells measured using flow cytometry. (Q) Schematic illustration of MAC-PNV-induced repolarization of M2 macrophages towards the M1 phenotype. Created with BioRender (https://biorender.com/). Data are represented as mean ± SD ($n = 3$). $^*P < 0.05$, $^{**}P < 0.01$, $^{***}P < 0.001$.

M2 TAMs towards M1 phenotype. Moreover, the highest intratumoral levels of pro-inflammatory cytokines (TNF-α, IFN-γ, and IL-6) were seen in MAC-PNV group (Fig. 6L–N). It was demonstrated that the robust $CD8^+$ T cell activation and TME remodeling effect of MAC-PNV were attributed to the increased cytokines predominantly secreted by M1 TAMs and activated $CD8^+$ T cells.

In addition to the effects evaluated on the primary tumor models, the therapeutic efficiency of MAC-PNV on distal tumors was also investigated in bilateral B16-OVA tumor-bearing C57BL/6J mice. The distal tumors were inoculated in the left flank on the 3rd day after subcutaneous inoculations of primary tumor cells into the right flank. On the 7th, 10th, and 13th days, PBS, DC-NV, MAC-CNV, and MAC-PNV were peritumorally injected into the primary tumor site, respectively (Supporting Information Fig. S13A). As shown in Fig. S13B and S13C, the significantly higher inhibition rates of 75.92% and 70.09% in primary and distal tumors were seen in MAC-PNV group than those in DC-NV (39.60% and 33.48%) and MAC-CNV (51.64% and 15.42%) groups. Consistent with these findings, the images of *ex vivo* tumor tissues (Fig. S13D and S13E) and the measurement of tumor weights (Fig. S13F and S13G) also demonstrated that the MAC-PNV group exhibited the strongest growth inhibition on both primary and distal tumors among all groups. To further elucidate the anti-tumor immune mechanisms, the infiltration of $CD8^+$ T cells and the percentage of M2 TAMs in primary and distal tumors, and the percentage of IFN-γ^+CD8^+ T cells in the spleen were investigated using flow cytometry. As shown in Fig. S13H–S13K, the MAC-PNV group exhibited the highest percentages of $CD8^+$ T cells (gated on $CD45^+CD3^+$) and the lowest percentages of M2 TAMs (gated on $CD11b^+$ $F4/80^+$) within both primary and distal tumors. In addition, the highest percentages of IFN-γ^+CD8^+ T cells in the spleens were found in the MAC-PNV group among all groups (Fig. S13L). These findings collectively indicated that MAC-PNV elicited a robust, systemic anti-tumor immune response. It was speculated that the $CD8^+$ T cell activation and pro-inflammatory cytokine production triggered by MAC-PNV in primary tumors would enhance the functions of $CD8^+$ T cells (*e.g.*, cytotoxic killing, IFN-γ production) and TME remodeling in distal tumors, along with promoting migration of activated $CD8^+$ T cells to distal tumors.

Taken together, these results demonstrated that MAC-PNV induced a potent anti-tumor immune response by promoting the activation and intra-tumoral infiltration of $CD8^+$ T cells, and remodeling the TME through repolarization of TAMs towards M1 phenotype. This synergistic immunomodulation effectively amplified the tumor-specific killing capability of $CD8^+$ T cells in remodeled TME, thereby resulting in robust tumor suppression in the B16-OVA melanoma model.

3.6. In vivo therapeutic efficacy of MAC-PNV combined with liposomal doxorubicin in B16-OVA tumor models

As a conventional chemotherapeutic agent, the liposomal doxorubicin (DOX-Lipo, *e.g.*, Doxil®) is always limited by insufficient therapeutic efficacy and dose-limiting systemic toxicities in the clinic[55]. Importantly, it had been demonstrated that the combination of immunotherapy with chemotherapy could achieve superior therapeutic outcomes compared to chemotherapy alone, with significant survival benefits in multiple clinical trials[56,57]. In this study, based on the significantly higher levels of IFN-γ, TNF-α, and IFN-γ^+CD8^+ T cells in tumor tissues induced by MAC-PNV (Fig. 6H, L, and M), the anti-tumor efficacy of DOX-Lipo combined with MAC-PNV was further investigated (Supporting Information Table S2 and Fig. S14). As shown in Fig. 7A, MAC-PNV (1 mg/mL of total protein, 100 μL per mouse) was injected peritumorally, and DOX-Lipo (3 mg/kg) was injected intravenously on the 7th, 10th, and 13th days in C57BL/6J mice bearing B16-OVA tumors. On the 13th day after treatment, the mice were euthanized, and the tumor weight and the immune-related indicators were measured. As shown in Fig. 7B, the significantly higher inhibition rate of tumor volume was seen in MAC-PNV + DOX-Lipo group (91.4%) than that in DOX-Lipo group (62.6%) and MAC-PNV group (69.6%). Furthermore, MAC-PNV + DOX-Lipo group exhibited a higher inhibition rate of tumor weight (93.02%), which was 1.35- and 1.23-fold higher than those of DOX-Lipo (68.78%) and MAC-PNV group (75.37%), respectively (Fig. 7C). Finally, the results of *ex vivo* tumor images demonstrated significantly stronger tumor inhibition effects in MAC-PNV + DOX-Lipo group than those in other groups (Fig. 7D). In addition, TUNEL immunofluorescence staining images revealed the highest level of tumor cell apoptosis (green signals) in the MAC-PNV + DOX-Lipo group (Fig. 7E). These results demonstrated that the combination treatment of MAC-PNV and DOX-Lipo (3 mg/kg) could achieve a stronger anti-tumor efficacy than single treatments.

To elucidate the immune-enhanced mechanisms of MAC-PNV for improving the anti-tumor effect of DOX-Lipo, the percentage of $CD80^+CD86^+$ population and SIINFEKL-H-$2Kb^+$ population among DCs in TDLNs, and the percentage of $CD8^+$ T cells in TDLNs and tumors were evaluated by flow cytometry. As shown in Fig. 7F and G, DOX-Lipo group showed higher percentages of $CD80^+CD86^+$ population (23.63%) and SIINFEKL-H-$2Kb^+$ population (12.43%) in DCs than those in PBS group (15.28% and 6.63%) in TDLNs, indicating that DOX-Lipo efficiently induced the DCs maturation and antigen presentation. Also, DOX-Lipo group showed significantly stronger CRT signals (red fluorescence) and markedly reduced intracellular HMGB1 signals (red fluorescence) than PBS group (Fig. 7H and I). It was demonstrated that the enhanced DC maturation and antigen presentation might be attributed to the DOX-induced immunogenic cell death (ICD) effect, which can efficiently promote the release of damage-associated molecular patterns and tumor antigens from tumor cells, thereby promoting DC activation[58]. Notably, the significantly higher percentages of $CD80^+CD86^+$ population (31.54%) and SIINFEKL-H-$2Kb^+$ population (18.68%) in DCs were found in the MAC-PNV + DOX-Lipo group than those in DOX-Lipo (23.63% and 12.43%) and MAC-PNV (19.80% and 7.72%) groups (Fig. 7F and G). As reported, the immunosuppressive TME can potently inhibit ICD-induced DCs activation through abnormal metabolism (*e.g.*, hypoxia, lactate accumulation) and immunosuppressive factors (*e.g.*, TGF-β)[59]. Therefore, the significantly stronger DCs activation achieved by the MAC-PNV + DOX-Lipo group might result from the immunosuppressive TME remodeling of MAC-PNV, followed by the DCs maturation and antigen presentation amplified by DOX-induced ICD. These activated DCs are critical for priming tumor-specific $CD8^+$ T cell responses. As shown in Fig. 7J and K, markedly increased percentages of $CD8^+$ T cells in TDLNs and tumor tissues were found in MAC-PNV + DOX-Lipo group, which were significantly higher than those in DOX-Lipo (1.33- and 1.47-fold) and MAC-PNV (1.1- and 1.27-fold) groups, respectively. The strongest effects of the MAC-PNV + DOX-Lipo combination on $CD8^+$ T cell activation and infiltration involved dual mechanisms:

direct enhancement of $CD8^+$ T cell activation by MAC-PNV, and the amplified DOX-Lipo-induced DCs activation after TME remodeling of MAC-PNV. Therefore, it was demonstrated that the improved therapeutic efficacy of MAC-PNV + DOX-Lipo combination on the primary B16-OVA tumor model was mainly due to the $CD8^+$ T cell activation and TME remodeling triggered by MAC-PNV.

Considering the excellent therapeutic efficacy on the primary B16-OVA tumor model, the anti-metastasis ability of MAC-PNV + DOX-Lipo combination was further evaluated in the B16-OVA lung metastases model. The lung metastasis models were established by intravenous injection of B16-OVA cells on the Day 0, along with subcutaneous inoculations of primary tumor models into the right flank in C57BL/6J mice. These mice were divided into four groups, including PBS, DOX-Lipo, MAC-PNV, and MAC-PNV + DOX-Lipo groups. MAC-PNV (1 mg/mL of total protein, 100 μL per mouse) was injected peritumorally, and DOX-Lipo (3 mg/kg) was injected intravenously on the 7th, 10th, and 13th days. After the mice were euthanized on the 23rd day, the lung tissues were excised for analyzing metastatic nodules (Fig. 7L). As shown in Fig. 7M and N, only 10 metastasis foci were observed in the lung tissues after MAC-PNV + DOX-Lipo treatment. A higher metastasis inhibition rate (calculated according to the count of metastasis nodules) was seen in the MAC-PNV + DOX-Lipo group (77.20%) compared to the DOX-Lipo (52.20%) and MAC-PNV (50.0%) groups (Fig. 7N). Also, H&E staining of lung sections indicated a significantly lower number of lung metastasis nodules in the MAC-PNV + DOX-Lipo group than in the other groups (Supporting Information Fig. S15). These results demonstrated that the combination with MAC-PNV could significantly enhance the anti-metastatic efficiency of DOX-Lipo. This significantly enhanced anti-metastatic activity of the combination therapy was likely due to the synergistic effects of DOX-Lipo-mediated cytotoxicity and MAC-PNV-activated $CD8^+$ T cells against tumor cells in systemic circulation.

Taken together, these findings demonstrated that MAC-PNV presenting $OVA_{257-264}$ could significantly enhance the anti-tumor efficacy of DOX-Lipo in both primary and metastatic B16-OVA tumor models. Considering that $OVA_{257-264}$ was a model antigenic peptide, another tumor-associated antigen presented by MAC-PNV was prepared and used to further evaluate the capability in enhancing anti-tumor efficacy of DOX-Lipo.

3.7. In vivo therapeutic efficacy of MAC-PNV$_{TRP2}$ combined with low-dose liposomal doxorubicin in B16-F10 tumor models

Tyrosinase-related protein 2 (TRP2) peptide-$TRP2_{181-188}$ is a melanoma-associated antigenic peptide conforming to the H-2Kb-restricted peptide epitope[60]. Previous studies had demonstrated that DCs presenting $TRP2_{181-188}$ could induce effective anti-tumor immunity[60]. In this study, $TRP2_{181-188}$ was used as the tumor antigenic peptide to prepare MAC-PNV_{TRP2}. Considering that MAC-PNV (presenting $OVA_{257-264}$) significantly enhanced the anti-tumor efficacy of DOX-Lipo at a dose of 3 mg/kg in B16-OVA-bearing mouse models, we next investigated whether combining MAC-PNV_{TRP2} (presenting $TRP2_{181-188}$) with a low-dose DOX-Lipo (1 mg/kg, DOX-Lipo(L)) could achieve potent anti-tumor activity and mitigate the dose-limiting toxicity associated with DOX-Lipo in B16-F10-bearing mouse models (Fig. 8A). These mice were divided into PBS, DOX-Lipo(L) (low-dose DOX, 1 mg/kg), DOX-Lipo (3 mg/kg), MAC-PNV_{TRP2}, MAC-PNV_{TRP2}+DOX-Lipo(L), and MAC-PNV_{TRP2}+DOX-Lipo groups. MAC-PNV_{TRP2} (1 mg/mL of total protein, 100 μL per mouse) was injected peritumorally, and DOX-Lipo was injected intravenously on the 7th, 10th, and 13th days. As shown in Fig. 8B and C, all combination treatments (MAC-PNV_{TRP2}+DOX-Lipo(L) and MAC-PNV_{TRP2}+DOX-Lipo groups) exhibited a significantly stronger anti-tumor efficacy than monotherapy groups. Notably, even though one-third dose of DOX (1 mg/kg) was injected, the tumor growth inhibition rate in the mice treated with DOX-Lipo(L) and MAC-PNV_{TRP2} was 78.65%, which was significantly higher than that in DOX-Lipo(L) (38.93%), DOX-Lipo (58.47%) and MAC-PNV_{TRP2} (61.25%), respectively (Fig. 8B). With the increase in dose of DOX, the tumor growth inhibition rate in MAC-PNV_{TRP2}+DOX-Lipo group was increased to 89.86% (Fig. 8B). These findings demonstrated that MAC-PNV_{TRP2} could significantly amplify the anti-tumor efficacy of DOX-Lipo even at the low dose (1 mg/kg), providing a promising immunomodulatory enhancer for chemotherapeutics.

To elucidate the underlying anti-tumor immune mechanism of the combination therapy in inhibiting the growth of B16-F10 tumors, the percentages of IFN-γ^+CD8^+ T cells in TDLNs, peripheral blood, and tumor tissues, as well as the ratio of M1/M2 TAMs within tumors, were detected by flow cytometry. As shown in Fig. 8D−F, the dramatic increases in the percentages of IFN-γ^+CD8^+ T cells in TDLNs were observed in MAC-PNV_{TRP2}+DOX-Lipo(L) (24.29%) and MAC-PNV_{TRP2}+DOX-Lipo (38.35%) groups, compared to DOX-Lipo(L) (3.21%), DOX-Lipo (3.16%), and MAC-PNV_{TRP2} (15.88%) groups. Furthermore, both combination groups exhibited significantly higher percentages of IFN-γ^+CD8^+ T cells in peripheral blood and tumor tissues relative to the monotherapy groups. These results indicated that combination therapy could potently induce $CD8^+$ T cells activation within TDLNs. These activated $CD8^+$ T cells subsequently migrated *via* the bloodstream and infiltrated tumor tissues, driving potent anti-tumor immunity. Additionally, a significantly higher ratio of M1/M2 TAMs was found in MAC-PNV_{TRP2}+DOX-Lipo(L) group (1.99) than that in DOX-Lipo(L) (0.52, $P < 0.05$) group, while no significant difference was observed compared to MAC-PNV_{TRP2} group (1.43, $P > 0.05$) (Fig. 8G), indicating that the pro-inflammatory shift was primarily driven by MAC-PNV_{TRP2}-mediated TAM reprogramming. Therefore, these results demonstrated that MAC-PNV_{TRP2} combined with low-dose DOX-Lipo (1 mg/kg) effectively induced a more potent anti-tumor immune response, leading to superior tumor growth inhibition.

To further evaluate the biosafety of the combination strategy, body weights, key parameters of hematology and biochemistry, and the levels of TNF-α and IL-6 in the serum were measured. As shown in Supporting Information Fig. S16, no significant changes in body weight of mice were observed in each group throughout the treatment period. Furthermore, the levels of LDH, CK, ALT, AST, CREA, and UREA remained unchanged in the serum of mice after treatment with different formulations compared to the PBS group (Fig. 8H and I, Supporting Information Fig. S17), indicating no detectable cardiotoxicity, hepatotoxicity, and nephrotoxicity at the administered dosage of DOX-Lipo (1 or 3 mg/kg). In addition, no significant differences were observed in serum levels of TNF-α and IL-6 between any treatment group and the PBS group (Supporting Information Fig. S18), suggesting that the treatments did not elicit systemic inflammation under the short-term treatment regimen. The analysis of complete blood counts revealed that comparable levels of RBC, PLT, and HGB were maintained among all treatment groups (Fig. 8J−L). Notably, mice treated with DOX-Lipo (3 mg/kg) exhibited significant

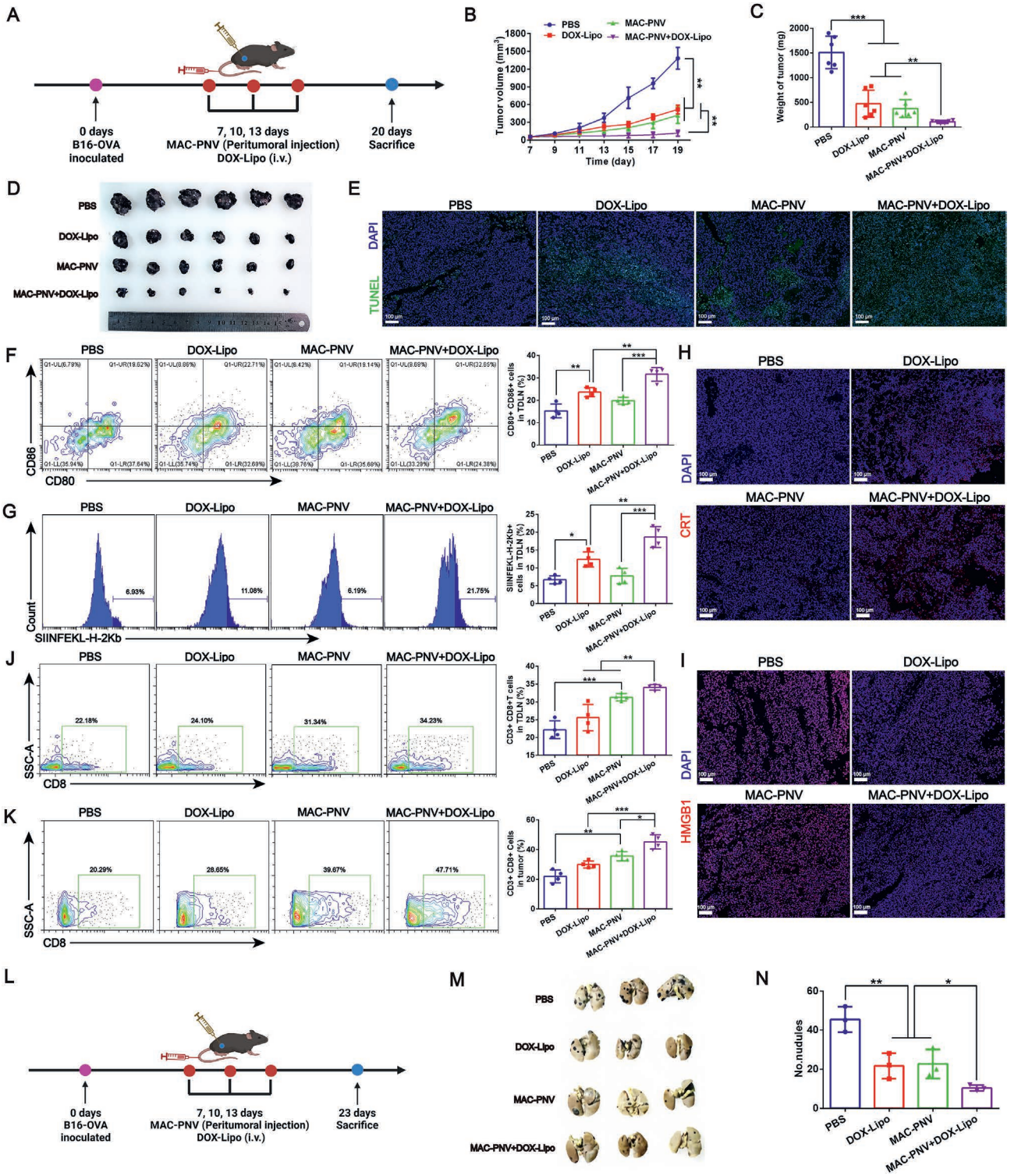

Figure 7 *In vivo* anti-tumor efficacy and immune responses of MAC-PNV combined with liposomal doxorubicin (DOX-Lipo, 3 mg/kg) in B16-OVA tumor models. (A) Schematic illustration of the experimental design. MAC-PNV was injected peritumorally, and DOX-Lipo was injected intravenously on the 7th, 10th, and 13th days, respectively. (B) Tumor growth curves of mice treated with different formulations ($n = 6$). (C) Tumor weights of mice after different treatments on the 20th day ($n = 6$). (D) *Ex vivo* tumor images of mice after different treatments on the 20th day ($n = 6$). (E) Representative immunofluorescence staining images of TUNEL (green) in tumor tissues. The nucleus was stained with DAPI (blue). Scale bars, 100 μm. (F) Representative flow cytometry plots and the percentage of $CD80^+CD86^+$ DCs (gated on $CD11c^+$) in TDLNs after different treatments ($n = 4$). (G) Representative flow cytometry plots and the percentage of $SIINFEKL\text{-}H\text{-}2Kb^+$ DCs (gated on $CD11c^+$) in TDLNs after different treatments ($n = 4$). Representative immunofluorescence staining images of (H) CRT (red), and (I) HMGB1 (red) in tumor tissues. The nucleus was stained with DAPI (blue). Scale bars, 100 μm. Representative flow cytometry plots and the percentage of $CD8^+$ T cells

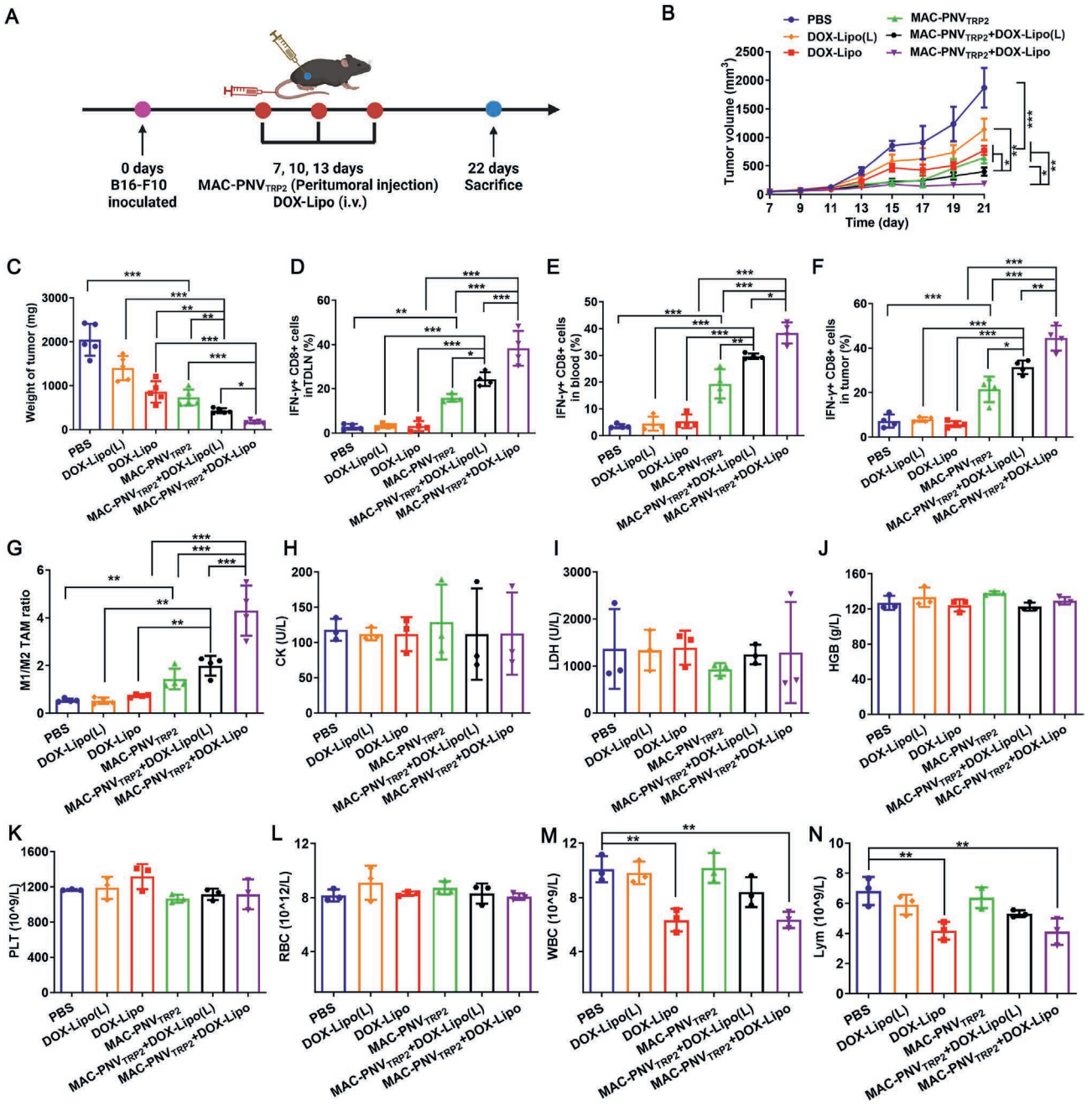

Figure 8 *In vivo* anti-tumor efficacy and immune responses of MAC-PNV$_{TRP2}$ combined with DOX-Lipo (1 or 3 mg/kg) in B16-F10 tumor models. (A) Schematic illustration of the experimental design. MAC-PNV$_{TRP2}$ was administered peritumorally, and DOX-Lipo was injected intravenously on the 7th, 10th, and 13th days. (B) Tumor growth curves of mice treated with different formulations ($n = 5$). (C) Tumor weights of mice after different treatments on Day 22 ($n = 5$). The percentage of IFN-γ^+CD8$^+$ T cells in (D) TDLNs, (E) peripheral blood, and (F) tumor tissues after different treatments ($n = 4$). (G) The ratios of M1/M2 TAMs after different treatments ($n = 4$). The levels of (H) creatine kinase (CK) and (I) LDH in the serum of mice treated with different formulations ($n = 3$). The levels of (J) hemoglobin (HGB), (K) platelets (PLT), (L) red blood cells (RBC), (M) white blood cells (WBC), and (N) lymphocytes (Lym) in the whole blood of mice treated with different formulations ($n = 3$). Data are represented as mean ± SD. *$P < 0.05$, **$P < 0.01$, ***$P < 0.001$.

(gated on CD3$^+$ CD45$^+$) in (J) TDLNs and (K) tumor tissues after different treatments ($n = 4$). (L) Schematic illustration of the experimental design of anti-lung metastasis. MAC-PNV were injected peritumorally, and DOX-Lipo was injected intravenously on the 7th, 10th, and 13th days, respectively. (M) *Ex vivo* lung images of mice treated with different formulations on the 23rd day ($n = 3$). (N) The number of lung metastasis nodules after different treatments ($n = 3$). Data are represented as mean ± SD. *$P < 0.05$, **$P < 0.01$, ***$P < 0.001$.

reductions in WBC and Lym counts (Fig. 8M and N), suggesting bone marrow suppression at this dose. In contrast, WBC and Lym counts in DOX-Lipo(L) and MAC-PNV$_{TRP2}$+DOX-Lipo(L) groups remained comparable to those in the PBS group, indicating no significant bone marrow suppression at the low dose of DOX-Lipo (1 mg/kg).

In summary, these results demonstrated that the combination therapy of MAC-PNV$_{TRP2}$ with a low-dose DOX-Lipo (1 mg/kg) could significantly amplify the anti-tumor efficacy and avoid the dose-limiting toxicity of DOX-Lipo. These findings demonstrated that MAC-PNV could be used as a general platform for presenting different antigens and highlighted its potential as an effective immunomodulatory enhancer for chemotherapeutics.

Although MAC-PNV exhibited great potential in anti-tumor immunotherapy, its clinical translation still faces several challenges, including scalable production, batch-to-batch quality control, and comprehensive immunogenicity assessment, as commonly encountered with cell-derived nanotherapeutics[61].

4. Conclusions

In this study, an engineered nanovesicle (MAC-PNV) integrating dual anti-tumor functionalities of robust CD8$^+$ T cell activation and immunosuppressive TME remodeling was successfully developed. Upon peritumoral administration, MAC-PNV alone exhibited significantly stronger anti-tumor effects compared to DC-NV and MAC-CNV. This enhanced efficacy was mediated not only by the direct activation of CD8$^+$ T cells upon drainage into TDLNs, but also by the polarization of M2 TAMs towards the pro-inflammatory M1 phenotype in tumors. Interestingly, combined with DOX-Lipo, MAC-PNV further amplified anti-tumor immunity and reduced dose-limiting toxicity of DOX, thereby synergistically achieving remarkable inhibitory effects on tumor growth and metastasis. It was believed that MAC-PNV could be used as an immune-enhancer for improving chemotherapeutic efficacy.

Acknowledgments

The work was supported by the projects of National Natural Science Foundation of China (Grant Nos. 81973259, U22A20384, 82574341, and 82173726), Beijing Natural Science Foundation (Grant No. L242056, China), Ningbo Science and Technology Plan Project (Grant No. 2022Z142, China), the excellent talent project of Peking University (Grant No. BMU2022XY024, China), and China Postdoctoral Science Foundation (Grant No 2025T180979).

Author contributions

Linxia Jiang: Writing-original draft, Validation, Methodology, Data curation, Conceptualization. Yi Yan: Writing-original draft, Validation, Methodology, Data curation, Conceptualization. Hongqian Xie: Methodology, Investigation. Zhiyi Xu: Methodology, Investigation. Xiaoru Guo: Methodology, Investigation. Jinyue Li: Methodology, Investigation. Xiaoyu Liu: Methodology, Investigation. Di Wu: Methodology, Investigation. Yuanjun Zhu: Writing-review & editing, Supervision. Yujie Shi: Writing-review & editing, Supervision. Xiaoyan Liu: Writing-review & editing, Supervision. Jian-Cheng Wang: Writing-review & editing, Visualization, Supervision, Project administration, Funding acquisition, Conceptualization.

Conflicts of interest

The authors declare no conflicts of interest.

Appendix A. Supporting information

Supporting information to this article can be found online at https://doi.org/10.1016/j.apsb.2025.12.029.

References

1. Zhang Y, Zhang Z. The history and advances in cancer immunotherapy: understanding the characteristics of tumor-infiltrating immune cells and their therapeutic implications. *Cell Mol Immunol* 2020;**17**:807−21.
2. Philip M, Schietinger A. CD8$^+$ T cell differentiation and dysfunction in cancer. *Nat Rev Immunol* 2022;**22**:209−23.
3. Wang XY, Yan Y, Guo XR, Lu A, Jiang LX, Zhu YJ, et al. Enhanced tumor immunotherapy by triple amplification effects of nanomedicine on the STING signaling pathway in dendritic cells. *Adv Healthcare Mater* 2025;**14**:e2403143.
4. Wan D, Bai Z, Zhang Y, Chen L, Que H, Lan T, et al. Simultaneous enhancement of cellular and humoral immunity by the lymph node-targeted cholesterolized TLR7 agonist liposomes. *Acta Pharm Sin B* 2024;**14**:4577−90.
5. Pitt JM, Marabelle A, Eggermont A, Soria JC, Kroemer G, Zitvogel L. Targeting the tumor microenvironment: removing obstruction to anticancer immune responses and immunotherapy. *Ann Oncol* 2016;**27**:1482−92.
6. Cassetta L, Pollard JW. A timeline of tumour-associated macrophage biology. *Nat Rev Cancer* 2023;**23**:238−57.
7. Wang S, Li F, Ye T, Wang J, Lyu C, Qing S, et al. Macrophage-tumor chimeric exosomes accumulate in lymph node and tumor to activate the immune response and the tumor microenvironment. *Sci Transl Med* 2021;**13**. eabb6981.
8. Pittet MJ, Di Pilato M, Garris C, Mempel TR. Dendritic cells as shepherds of T cell immunity in cancer. *Immunity* 2023;**56**:2218−30.
9. Rosa FF, Pires CF, Kurochkin I, Ferreira AG, Gomes AM, Palma LG, et al. Direct reprogramming of fibroblasts into antigen-presenting dendritic cells. *Sci Immunol* 2018;**3**. eaau4292.
10. Zimmermannova O, Ferreira AG, Ascic E, Velasco Santiago M, Kurochkin I, Hansen M, et al. Restoring tumor immunogenicity with dendritic cell reprogramming. *Sci Immunol* 2023;**8**. eadd4817.
11. Ascic E, Akerstrom F, Sreekumar Nair M, Rosa A, Kurochkin I, Zimmermannova O, et al. *In vivo* dendritic cell reprogramming for cancer immunotherapy. *Science* 2024;**386**. eadn9083.
12. Rosa FF, Pires CF, Kurochkin I, Halitzki E, Zahan T, Arh N, et al. Single-cell transcriptional profiling informs efficient reprogramming of human somatic cells to cross-presenting dendritic cells. *Sci Immunol* 2022;**7**. eabg5539.
13. Xiang X, Wang J, Lu D, Xu X. Targeting tumor-associated macrophages to synergize tumor immunotherapy. *Signal Transduct Targeted Ther* 2021;**6**:75.
14. Li C, Xu X, Wei S, Jiang P, Xue L, Wang J, et al. Tumor-associated macrophages: potential therapeutic strategies and future prospects in cancer. *J Immunother Cancer* 2021;**9**:e001341.
15. Choo YW, Kang M, Kim HY, Han J, Kang S, Lee JR, et al. M1 Macrophage-derived nanovesicles potentiate the anticancer efficacy of immune checkpoint inhibitors. *ACS Nano* 2018;**12**:8977−93.
16. Zhen X, Li Y, Yuan W, Zhang T, Li M, Huang J, et al. Biointerface-engineered hybrid nanovesicles for targeted reprogramming of tumor microenvironment. *Adv Mater* 2024;**36**:e2401495.

17. Neupane KR, Ramon GS, Harvey B, Chun B, Aryal SP, Masud AA, et al. Programming cell-derived vesicles with enhanced immunomodulatory properties. *Adv Healthcare Mater* 2023;**12**:e2301163.
18. Wang W, li J, Wu K, Azhati B, Rexiati M. Culture and identification of mouse bone marrow-derived dendritic cells and their capability to induce T lymphocyte proliferation. *Med Sci Monit* 2016;**22**:244−50.
19. Zheng X, Jiang Q, Han M, Ye F, Wang M, Qiu Y, et al. FBXO38 regulates macrophage polarization to control the development of cancer and colitis. *Cell Mol Immunol* 2023;**20**:1367−78.
20. Santos MM, Samba M, Layoun A. Isolation of murine peritoneal macrophages to carry out gene expression analysis upon toll-like receptors stimulation. *J Vis Exp* 2015;**29**:e52749.
21. Yao RF, Luo YY, Tian HL. Hypoxia-derived mesenchymal stem-cell exosomes delivering naringin enhance osteoblast migration and fracture healing by upregulating integrin *β1 via* the BDNF−TrkB/ERK1/2 signaling pathway. *Eur Cell Mater* 2025;**50**:137−51.
22. Liu L, Huang G, Bai H, Tang G. Synthesis of folate modified chitosan-based nanomicelles and its *in vitro* anti-tumor activity. *Zhejiang Da Xue Xue Bao Yi Xue Ban* 2020;**49**:364−74.
23. Guo Y, Hu G, Xia Y, Li H, Yuan J, Zhang J, et al. Eliminating the original cargos of glioblastoma cell-derived small extracellular vesicles for efficient drug delivery to glioblastoma with improved biosafety. *Bioact Mater* 2022;**16**:204−17.
24. Lin S, Shu L, Guo Y, Yuan J, Zhang J, Wang Y, et al. Cargo-eliminated osteosarcoma-derived small extracellular vesicles mediating competitive cellular uptake for inhibiting pulmonary metastasis of osteosarcoma. *J Nanobiotechnol* 2024;**22**:360.
25. Gardner A, Ruffell B. Dendritic cells and cancer immunity. *Trends Immunol* 2016;**37**:855−65.
26. Tang-Huau TL, Gueguen P, Goudot C, Durand M, Bohec M, Baulande S, et al. Human *in vivo*-generated monocyte-derived dendritic cells and macrophages cross-present antigens through a vacuolar pathway. *Nat Commun* 2018;**9**:2570.
27. Lee CYC, Kennedy BC, Richoz N, Dean I, Tuong ZK, Gaspal F, et al. Tumour-retained activated CCR7(+) dendritic cells are heterogeneous and regulate local anti-tumour cytolytic activity. *Nat Commun* 2024;**15**:682.
28. Sun Z, Liu J, Li Y, Lin X, Chu Y, Wang W, et al. Aggregation-induced-emission photosensitizer-loaded nano-superartificial dendritic cells with directly presenting tumor antigens and reversed immunosuppression for photodynamically boostedimmunotherapy. *Adv Mater* 2023;**35**:e2208555.
29. Zhou F, Mei J, Han X, Li H, Yang S, Wang M, et al. Kinsenoside attenuates osteoarthritis by repolarizing macrophages through inactivating NF-kappaB/MAPK signaling and protecting chondrocytes. *Acta Pharm Sin B* 2019;**9**:973−85.
30. He T, Tang C, Xu S, Moyana T, Xiang J. Interferon gamma stimulates cellular maturation of dendritic cell line DC2.4 leading to induction of efficient cytotoxic T cell responses and antitumor immunity. *Cell Mol Immunol* 2007;**4**:105−11.
31. Yan Y, Lu A, Dou Y, Zhang Z, Wang XY, Zhai L, et al. Nanomedicines reprogram synovial macrophages by scavenging nitric oxide and silencing CA9 in progressive osteoarthritis. *Adv Sci (Weinh)* 2023;**10**:e2207490.
32. Hogquist KA, Jameson SC, Heath WR, Howard JL, Bevan MJ, Carbone FR. T cell receptor antagonist peptides induce positive selection. *Cell* 1994;**76**:17−27.
33. Wen Y, Fu Q, Soliwoda A, Zhang S, Zheng M, Mao W, et al. Cell-derived nanovesicles prepared by membrane extrusion are good substitutes for natural extracellular vesicles. *Extracell Vesicle* 2022;**1**:100004.
34. Qiu C, Zhao Z, Xu C, Yuan R, Ha Y, Tu Q, et al. Nebulized milk exosomes loaded with siTGF-beta1 ameliorate pulmonary fibrosis by inhibiting EMT pathway and enhancing collagen permeability. *J Nanobiotechnol* 2024;**22**:434.
35. Lu A, Du K, Wang M, Zhu Z, Lei L, Shi Y. Natural endogenous material-based vehicles for delivery of macromolecular drugs. *Chin J Nat Med* 2024;**22**:1163−76.
36. Li W, Zhang H, Chen L, Huang C, Jiang Z, Zhou H, et al. Cell membrane-derived nanovesicles as extracellular vesicle-mimetics in wound healing. *Mater Today Bio* 2025;**31**:101595.
37. Shah K, Al-Haidari A, Sun J, Kazi JU. T cell receptor (TCR) signaling in health and disease. *Signal Transduct Targeted Ther* 2021;**6**:412.
38. Shen J, Xiao Z, Zhao Q, Li M, Wu X, Zhang L, et al. Anti-cancer therapy with TNFalpha and IFNgamma: a comprehensive review. *Cell Prolif* 2018;**51**:e12441.
39. Niederlova V, Tsyklauri O, Kovar M, Stepanek O. IL-2-driven CD8(+) T cell phenotypes: implications for immunotherapy. *Trends Immunol* 2023;**44**:890−901.
40. Binnewies M, Roberts EW, Kersten K, Chan V, Fearon DF, Merad M, et al. Understanding the tumor immune microenvironment (TIME) for effective therapy. *Nat Med* 2018;**24**:541−50.
41. Pollard JW. Tumour-educated macrophages promote tumour progression and metastasis. *Nat Rev Cancer* 2004;**4**:71−8.
42. Ngambenjawong C, Gustafson HH, Pun SH. Progress in tumor-associated macrophage (TAM)-targeted therapeutics. *Adv Drug Deliv Rev* 2017;**114**:206−21.
43. Liu D, Liang S, Ma K, Meng QF, Li X, Wei J, et al. Tumor microenvironment-responsive nanoparticles amplifying STING signaling pathway for cancer immunotherapy. *Adv Mater* 2024;**36**:e2304845.
44. Wang S, Wang J, Chen Z, Luo J, Guo W, Sun L, et al. Targeting M2-like tumor-associated macrophages is a potential therapeutic approach to overcome antitumor drug resistance. *npj Precis Oncol* 2024;**8**:31.
45. Wang H, Wang X, Zhang X, Xu W. The promising role of tumor-associated macrophages in the treatment of cancer. *Drug Resist Updates* 2024;**73**:101041.
46. Wang R, Zhu Z, Peng S, Xu J, Chen Y, Wei S, et al. Exosome microRNA-125a-5p derived from epithelium promotes M1 macrophage polarization by targeting IL1RN in chronic obstructive pulmonary disease. *Int Immunopharmacol* 2024;**137**:112466.
47. Cheng J, Tian X, Wu C, Wang J, Liu H, Cheng S, et al. MiR- 146b-5p inhibits Candida albicans-induced inflammatory response through targeting HMGB1 in mouse primary peritoneal macrophages. *Heliyon* 2025;**11**:e41464.
48. Wang Y, Han Z, Fan Y, Zhang J, Chen K, Gao L, et al. MicroRNA-9 inhibits NLRP3 inflammasome activation in human atherosclerosis inflammation cell models through the JAK1/STAT signaling pathway. *Cell Physiol Biochem* 2017;**41**:1555−71.
49. Zheng Z, Cao F, Ding YX, Lu JD, Fu YQ, Liu L, et al. Acinous cell AR42J-derived exosome miR125b-5p promotes acute pancreatitis exacerbation by inhibiting M2 macrophage polarization *via* PI3K/AKT signaling pathway. *World J Gastrointest Surg* 2023;**15**:600−20.
50. Zhang F, Parayath NN, Ene CI, Stephan SB, Koehne AL, Coon ME, et al. Genetic programming of macrophages to perform anti-tumor functions using targeted mRNA nanocarriers. *Nat Commun* 2019;**10**:3974.
51. Xu H, Zhu J, Smith S, Foldi J, Zhao B, Chung AY, et al. Notch-RBP-J signaling regulates the transcription factor IRF8 to promote inflammatory macrophage polarization. *Nat Immunol* 2012;**13**:642−50.
52. Qian F, Deng J, Lee YG, Zhu J, Karpurapu M, Chung S, et al. The transcription factor PU.1 promotes alternative macrophage polarization and asthmatic airway inflammation. *J Mol Cell Biol* 2015;**7**:557−67.
53. Shin HE, Han JH, Shin S, Bae GH, Son B, Kim TH, et al. M1-polarized macrophage-derived cellular nanovesicle-coated lipid nanoparticles for enhanced cancer treatment through hybridization of gene therapy and cancer immunotherapy. *Acta Pharm Sin B* 2024;**14**:3169−83.
54. Kang JH, Zappasodi R. Modulating Treg stability to improve cancer immunotherapy. *Trends Cancer* 2023;**9**:911−27.
55. Rafiyath SM, Rasul M, Lee B, Wei G, Lamba G, Liu D. Comparison of safety and toxicity of liposomal doxorubicin *vs.* conventional anthracyclines: a meta-analysis. *Exp Hematol Oncol* 2012;**1**:10.

56. Emens LA, Middleton G. The interplay of immunotherapy and chemotherapy: harnessing potential synergies. *Cancer Immunol Res* 2015;**3**:436−43.
57. Wang L, He S, Liu R, Xue Y, Quan Y, Shi R, et al. A pH/ROS dual-responsive system for effective chemoimmunotherapy against melanoma *via* remodeling tumor immune microenvironment. *Acta Pharm Sin B* 2024;**14**:2263−80.
58. Kim M, Lee JS, Kim W, Lee JH, Jun BH, Kim KS, et al. Aptamer-conjugated nano-liposome for immunogenic chemotherapy with reversal of immunosuppression. *J Control Release* 2022;**348**:893−910.
59. Zhao C, Wang C, Shan W, Wang Z, Chen X, Deng H. Nanomedicines for an enhanced immunogenic cell death-based *in situ* cancer vaccination response. *Acc Chem Res* 2024;**57**:905−18.
60. Zhuang X, Wu T, Zhao Y, Hu X, Bao Y, Guo Y, et al. Lipid-enveloped zinc phosphate hybrid nanoparticles for codelivery of H-2K(b) and H-2D(b)-restricted antigenic peptides and monophosphoryl lipid A to induce anti-tumor immunity against melanoma. *J Control Release* 2016;**228**:26−37.
61. Zhang E, Phan P, Zhao Z. Cellular nanovesicles for therapeutic immunomodulation: a perspective on engineering strategies and new advances. *Acta Pharm Sin B* 2023;**13**:1789−827.